

A STUDY OF THE REGULARITY OF AUTOCORRELATION
OF MANIPULATION OF WRIST MOTION DURING EATING

A Thesis
Presented to
the Graduate School of
Clemson University

In Partial Fulfillment
of the Requirements for the Degree
Master of Science
Electrical Engineering

by
Xueting Yu
December 2014

Accepted by:
Dr. Adam W. Hoover, Committee Chair
Dr. Richard E. Groff
Dr. Eric R. Muth

Abstract

This thesis considers the problem of detecting the eating activities (e.g. meals, snacks) of people by tracking their wrist motion. Our goal is to automatically detect the start and end times of eating activities during free-living. It builds upon previous work done by our research group [6] [7] [8] [21]. The detection is done by segmenting data into segments then classifying the segments as EA (eating activity) and NonEA (non-eating activity) using a Bayesian classifier. Previous features used in the classifier developed by our group included the sum of acceleration, the amount of manipulation, the amount of wrist roll and the regularity of wrist roll [6] [7] [8]. Additional features studied include a frequency analysis of manipulation, the time since the last EA, and the cumulative time spent eating in a day [21]. In this thesis we study two new features: the autocorrelation of the manipulation and the off-line analysis of the time since the last EA. The autocorrelation feature enables the study of patterns of manipulation that may not be precisely regular, and facilitates frequency analysis through the transform of the manipulation signal into something more sinusoidal. The off-line analysis of the time since the last EA allows for the calculation of every possible combination of segment classifications throughout the day, so that an early incorrect classification of a segment as an EA does not always inadvertently affect the classification of subsequent segments. This thesis further discusses these concepts and then tests them under the framework developed by our group. The

overall accuracy of regularity of autocorrelation of manipulation along with the original 4 features is 70%. The overall accuracy of trying every combination along with the original 4 features is 65%. Finally, we compare the results to the previous work and discuss the results based on our findings.

Acknowledgments

I would like to express the deep appreciation to my adviser Dr. Adam Hoover, for allowing me the opportunity to participate in this meaningful project and for teaching me how to conduct research and disseminate findings. Without his guidance and persistent help, this thesis would not have been possible. I thank Dr. Groff and Dr. Muth, for giving of their time and energy to serve on my graduate committee.

Table of Contents

Title Page	i
Abstract	ii
Acknowledgments	iv
List of Tables	vi
List of Figures	vii
1 Introduction	1
1.1 Obesity and overweight	1
1.2 Tools for monitoring energy intake	2
1.3 Previous work of our group	3
1.4 Novelty	4
2 Methods	5
2.1 Overview	5
2.2 Data collection	15
2.3 New features	16
2.4 Software tool	26
2.5 Evaluation metrics	28
3 Results	30
3.1 Accuracy results	30
3.2 Regularity of autocorrelation of manipulation	33
3.3 Time since last EA	41
4 Discussion	45
Bibliography	47

List of Tables

2.1	Average feature values found during training. The values of features f_1, f_2, f_3 and f_4 were computed in [8]. The values of feature f_5 were computed independently for 2 data sets in [21]; the values given here are averaged across all data.	14
2.2	The factor values of different frequency ranges for data set 1, data set 2, and both data sets.	22
2.3	Statistics for regularity of autocorrelation of manipulation (both sets).	22
2.4	Keyboard commands of the software tool.	26
3.1	Results for previous features using average on all data [8].	30
3.2	Results of original 4 features (f_1, f_2, f_3, f_4) with the regularity of autocorrelation of manipulation feature (f_8), and trying every possible combination approach on the time since last EA (f_6) feature for each person in data Set 1.	31
3.3	Results of original 4 features (f_1, f_2, f_3, f_4) with the regularity of autocorrelation of manipulation feature (f_8), and trying every possible combination approach on the time since last EA (f_6) feature for each person in data Set 2.	32
3.4	Results of original 4 features (f_1, f_2, f_3, f_4) with the regularity of autocorrelation of manipulation feature (f_8), and trying every possible combination approach on the time since last EA (f_6) feature.	32

List of Figures

2.1	Raw data obtained from sensors over a period of 2 minutes from 13:37 to 13:39 (24 hour format).	6
2.2	Smoothed data in Figure 2.1 using Equation 2.1.	6
2.3	An example of sum of acceleration of a person over an entire day. Arrows indicate start and end of the meals/snacks.	8
2.4	Peak-based segmentation on Figure 2.3. Arrows indicate detected peaks. Segments are considered as periods between peaks.	8
2.5	The cumulative distribution function for each minute since last EA.	13
2.6	The averages and standard deviations of cumulative eating time for each minute since beginning recording.	13
2.7	Manipulation (top) with its autocorrelation (bottom).	16
2.8	FFT results of the manipulation (top 2 figures) and FFT results of the autocorrelation (bottom 2 figures) for Figure 2.7a and Figure 2.7b. After autocorrelation, the FFT result shows a higher concentration of power in a smaller range.	20
2.9	Distribution of regularity of autocorrelation of manipulation in frequency range $[\frac{3}{60}\text{Hz} - \frac{10}{60}\text{Hz}]$ (both sets). $X_{EA} = 1.324$, $X_{NonEA} = 4.024$	21
2.10	The flowchart of the algorithm of finding the combination with the max sum of probabilities.	25
2.11	Screenshot of the software tool.	27
3.1	The classification results of original 4 features for person ID 011. The ground truth EA segment is marked by downward arrows. The horizontal bars represent the segments that were classified as EA segment.	34
3.2	The classification results of original 4 features with regularity of autocorrelation of manipulation feature for person ID 011. The ground truth EA segment is marked by downward arrows. The horizontal bars represent the segments that were classified as EA segment.	34
3.3	Autocorrelation of manipulation for an EA segment located on the right-most position of the distribution of EA in Figure 2.9.	36
3.4	Autocorrelation of manipulation for a NonEA segment located on the left tail of the distribution of NonEA in Figure 2.9.	36
3.5	Autocorrelation of manipulation for an EA segment located in the area where the EA distribution overlaps the NonEA distribution in Figure 2.9.	37

3.6	Autocorrelation of manipulation for a NonEA segment located in the area where the NonEA distribution overlaps the EA distribution in Figure 2.9.	37
3.7	The manipulation of the EA segment in Figure 3.5. The EA segment spans 8 minutes.	38
3.8	An example of the autocorrelation of manipulation for an EA segment which shows the different periodicity between the begin and the end of the segment.	40
3.9	The manipulation of the EA segment in Figure 3.8	40
3.10	The classification results of the original 4 features for person ID 024. The ground truth EA segment is marked by downward arrows. The horizontal bars represent the segments that were classified as EA. . .	42
3.11	The classification results of trying every possible combination on the time since last EA feature with the original 4 features for person ID 024. The ground truth EA segment is marked by downward arrows. The horizontal bars represent the segments that were classified as EA. . .	42
3.12	The classification results of the original 4 features for person ID 001. The ground truth EA segments are marked by downward arrows. The horizontal bars represent the segments that were classified as EA. . .	43
3.13	The classification results of trying every possible combination on the time since last EA feature with the original 4 features for person ID 001. The ground truth EA segments are marked by downward arrows. The horizontal bars represent the segments that were classified as EA. . .	43

Chapter 1

Introduction

This thesis considers the problem of detecting the eating activities (e.g. meals, snacks) of people by tracking their wrist motion. On average, people eat 3-5 meals and snacks per day [1]. Our goal is to automatically detect the start and end times of each eating activity (EA) during free-living. We assume that the person is wearing a watch-like configuration of accelerometers and gyroscopes [8]. The sensors in the device continuously track the wrist motion. We are developing methods to process and analyze the sensor data obtained from the device in order to detect the EAs.

1.1 Obesity and overweight

The motivation is obesity. Obesity and overweight are critical public health issues in the United States and worldwide. It is estimated that in the United States, 17% children and 32% adults are overweight (body mass index > 25), and 2.8% of males and 6.9% of females are extremely obese (body mass index ≥ 40) [19]. In the past 30 years, the prevalence rate of obesity has undergone a sustained increase, with the world rate doubling since 1980 [13].

Obesity can contribute to several health risk factor for individuals, such as cardiovascular disease, diabetes, musculoskeletal disorders and cancers [26]. Overweight and obesity have also been linked to an increased risk of death [10]. In the U.S., the economic burden of obesity costs approximately 78.5 billion dollars and accounted for about nine percent of the total U.S. medical expenditures in 1998 [9].

The major cause of overweight and obesity is that energy intake and energy expenditure are not equal, which can be due to an increased intake of energy from food or insufficient physical activity [11]. There are numerous behavior changes that have been associated with improvements in the obesity and overweight conditions, such as a reduction in the consumption of fat and sugar, engaging in more physical activity, and a healthier life regime [24]. Self-monitoring has been consistently found to play a role in successful weight loss and weight management [3].

1.2 Tools for monitoring energy intake

Doubly-labeled water (DLW) is regarded as the gold standard measure for energy intake assessment with a reported precision of $\pm 3\%$ to 5% [22]. Carbon dioxide and water are produced during energy expenditure procedure. The DLW method can measure energy expenditure by calculating the difference between the isotope rates of hydrogen and oxygen [23]. However, the cost, expense and technical expertise required to administer DLW are large, so it is usually used only in studies with small sample sizes.

The three most common methods developed for the purpose of assessing energy intake are the diary record, 24 hour recall and food frequency questionnaire (FFQ) [25]. Diary record methods require the subject to record the details of foods and beverages consumed, preferably measured using scale devices or pre-packaged

quantities. Other information of the food including the brand names and cooking details should also be recorded [25]. Due to the user burden, seven days or less of recording is a typical interval. Although the diary record method does not require recall, the different eating habits of people could make it potentially less precise [15]. Burrows reported that 19%-41% error per day for the food record method were observed when comparing it to the DLW method [4]. The second method is the 24 hour recall, which is where individuals are interviewed about food and beverage consumption in the past 24 hours. Although it has less cost and burden, the 24 hour recall method is memory based and people have the tendency to underreport food consumption. Champagne et al., estimated 10%-30% food consumption underreporting in normal weight individuals and 20%-50% food consumption underreporting in obese individuals [5]. The third method reports the frequency of food and beverage consumption over a reference period (e.g. 6 months or a year) using a food frequency questionnaires. FFQs are used to identify food patterns or investigate associations between diet and disease, but are not designed to produce measures of energy intake and do not provide meal pattern information [27].

1.3 Previous work of our group

The work in this thesis is based on the previous work of our group [8] [21]. The goal is to automatically detect EAs during free-living using a watch-like device to continuously track the subject's wrist motion for an entire day [8]. The original features used in the classification algorithm are amount of wrist roll motion, regularity of wrist roll motion, linear acceleration and manipulation. Our group later studied the regularity of manipulation, the time since the last EA, and cumulative eating time. These features were computed using the sensor data obtained from the accelerometers

and gyroscopes in the watch-like device. The detection was done by segmenting data into segments then classifying the segments as EA and NonEA using a Bayesian classifier.

1.4 Novelty

We consider a new feature related to the regularity of manipulation [21]. The previous work analyzed the manipulation signal as a function of its sinusoidal components. However, if we explore deeper into the data, we find that the manipulation signal is not sinusoidal in form and is not strictly cyclical. In this thesis we studied the autocorrelation of the manipulation signal to transform it into something more sinusoidal. In addition, the previous work used the time-based features in the same framework as other features. In this framework, every segment was classified independently. However, time-based features must be dependent upon the classification of previous segments, causing a cascade effect in the classification output. In this thesis, we reexamine the time since last EA feature in a framework that tries every possible combination of EA and NonEA for all segments.

Chapter 2

Methods

Firstly, we overview the algorithm and the features previously developed by our group [6] [7] [8] [21]. We then describe the method of data collection. Next, we define the new features developed for this thesis. Finally, we introduce the software tool built for observing data and the evaluation metrics used to determine the accuracy of this approach.

2.1 Overview

Our method assumes a person is wearing a watch-like configuration of accelerometers and gyroscopes [8]. The sensors in the device track the linear and rotational motion of person's wrist. Figure 2.1 shows a sample of the data using a custom software tool developed for this work (it will be further described in section 2.4). From top to bottom we can see the data from accelerometers ($AccX$, $AccY$, $AccZ$)¹ and gyroscopes (Yaw , $Pitch$, $Roll$).

As Figure 2.1 illustrates, the raw data obtained from the sensors are noisy. A

¹ $AccX$ means acceleration in x direction.

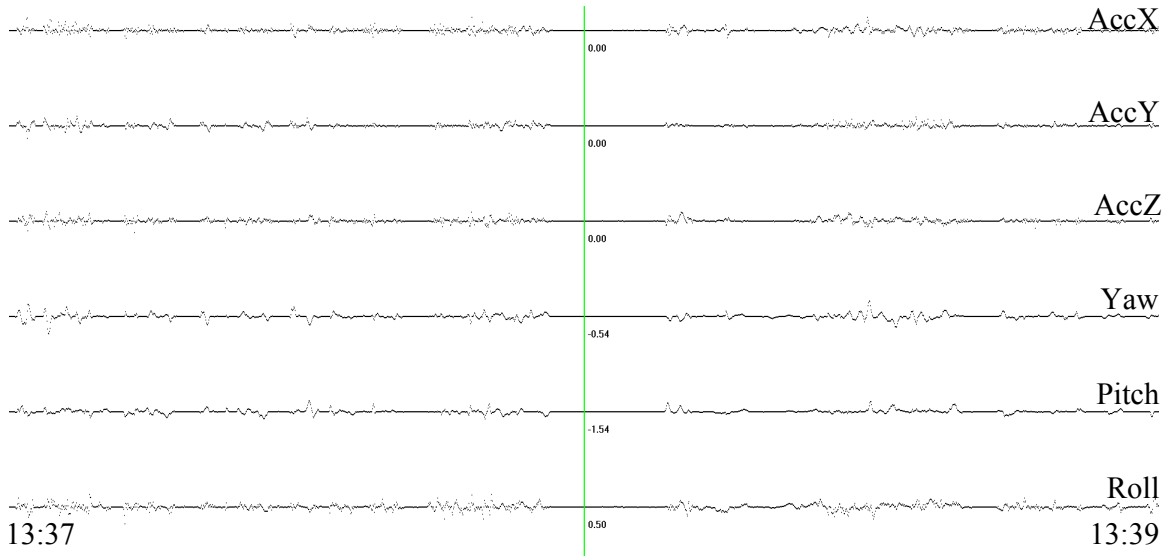


Figure 2.1: Raw data obtained from sensors over a period of 2 minutes from 13:37 to 13:39 (24 hour format).

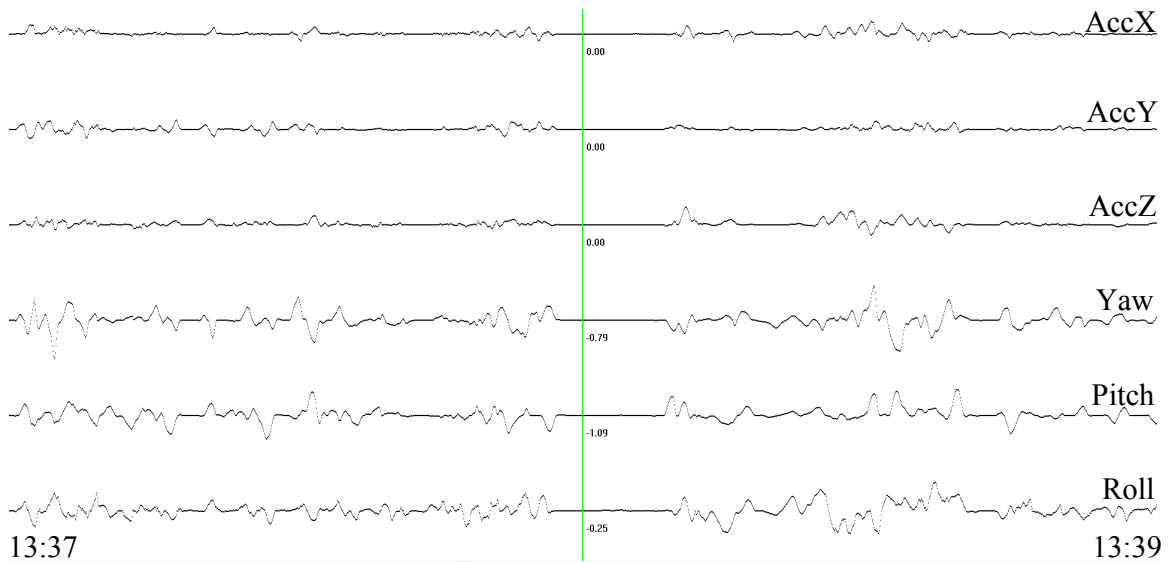


Figure 2.2: Smoothed data in Figure 2.1 using Equation 2.1.

Gaussian-weighted window is applied to reduce the effects of noise:

$$S_t = \sum_{i=-N}^0 R_{t+i} \frac{\exp(\frac{-t^2}{2R^2})}{\sum_{x=0}^N \exp(\frac{-(x-N)^2}{2R^2})} \quad (2.1)$$

where R_t is the obtained raw sensor data and S_t is the corresponding smoothed datum at time t . The Gaussian-weighted window implemented in Equation 2.1 centers on the current measurement, which means only half of a Gaussian distribution is used for smoothing. N represents the window size and R is the standard deviation of the Gaussian distribution. Equation 2.1 is applied independently to the data obtained from each accelerometer and gyroscope axis. Figure 2.2 shows the smoothed result of each axis for the raw sensor data shown in Figure 2.1. It is clear to see that data in Figure 2.2 is much smoother than raw sensor data in Figure 2.1.

In previous work our group found that there tends to be a period of larger wrist motion energy prior to an EA (caused by things like bringing food to a table, unwrapping food, adjusting the position of utensils, etc.), as well as at the end of an EA (caused by motions such as cleaning up a table, washing hands, standing up, etc.) [8]. Using this discovery, a method using the wrist motion energy was developed to perform data segmentation. Wrist motion energy as a feature is called sum of acceleration and is defined as follows:

$$E_t = \frac{1}{W+1} \sum_{i=t-\frac{W}{2}}^{t+\frac{W}{2}} |S_{x,t}| + |S_{y,t}| + |S_{z,t}| \quad (2.2)$$

where $S_{x,t}$, $S_{y,t}$ and $S_{z,t}$ are the smoothed acceleration readings at time t and W represents the window size. Our group has found that a sliding 1 minute window is sufficient for smoothing over short periods of large wrist motion while still capturing longer periods of vigorous motion which indicate the boundaries of an EA [8].

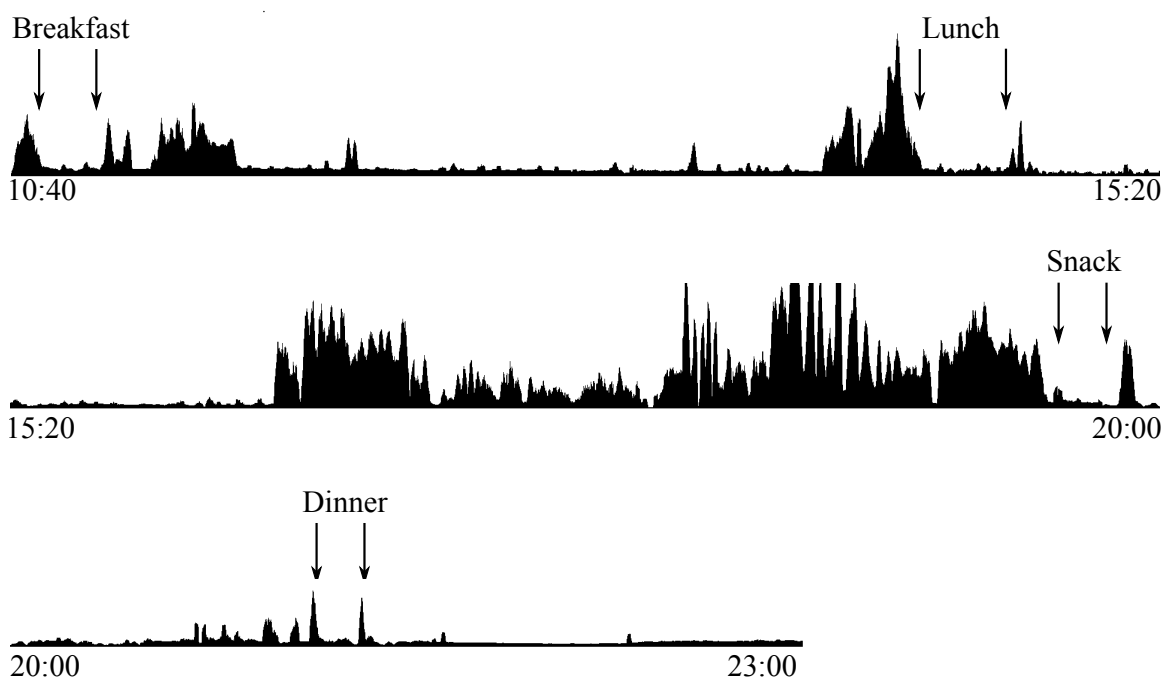


Figure 2.3: An example of sum of acceleration of a person over an entire day. Arrows indicate start and end of the meals/snacks.

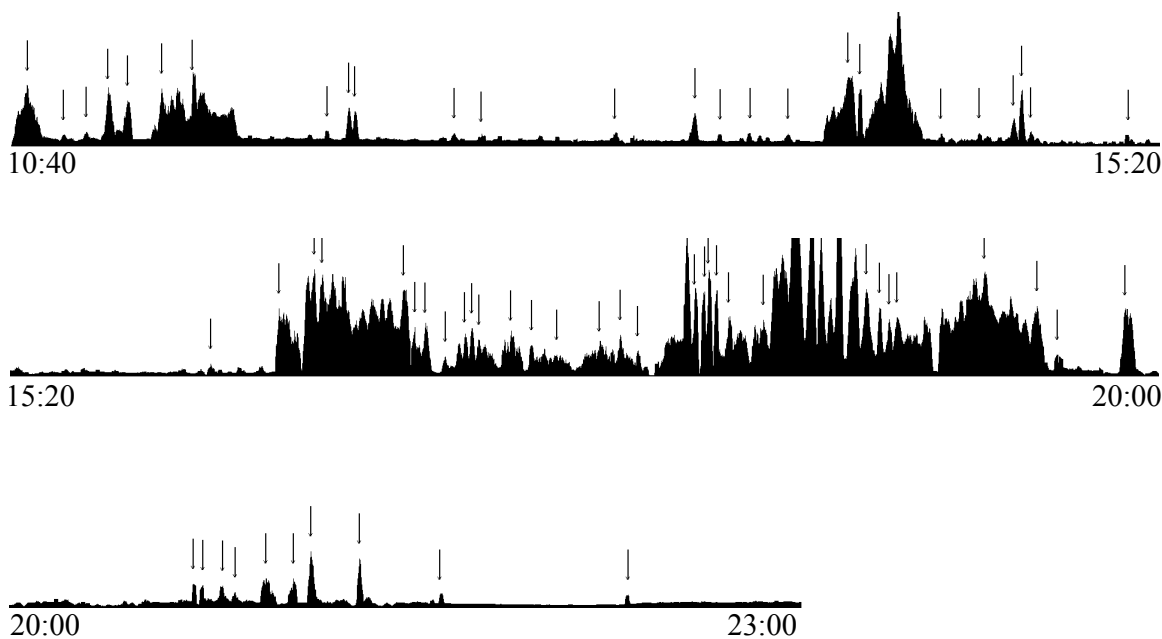


Figure 2.4: Peak-based segmentation on Figure 2.3. Arrows indicate detected peaks. Segments are considered as periods between peaks.

Figure 2.3 shows an example of sum of acceleration of a person for an entire day. The recording started at 10:40 and ended at 23:00. Meals and snack are indicated as downward arrows with the description of the EA (e.g. breakfast, snack, etc). The start and end times for each EA were manually recorded by the person wearing the watch-like configuration. Figure 2.3 illustrates that the sum of acceleration tends to be high before an EA begins as well as after it ends, and tends to be low during the period of the EA.

The data is segmented based on the sum of acceleration by automatically detecting peaks using a peak-based segmentation algorithm [8]. Figure 2.4 shows the result of performing automatically peak-based segmentation on the data in Figure 2.3. Arrows in the figure 2.4 indicate detected peaks. Segments are taken as all periods between two peaks (indices of arrows).

The original method developed by our group [8] used 4 features to classify segments. Each feature is computed over each detected segment (denoting as w). The first feature is manipulation. The manipulation measures the ratio of rotational wrist motion (*Yaw*, *Pitch* and *Roll*) to linear wrist motion (*AccX*, *AccY*, *AccZ*). It is calculated as:

$$f_1 = \frac{1}{W} \sum^W \frac{|S_{\phi,t}| + |S_{\theta,t}| + |S_{\psi,t}|}{|S_{x,t}| + |S_{y,t}| + |S_{z,t}|} \quad (2.3)$$

where W is the span of the segment period, t is the index that iterates across the span, and S is the smoothed datum (ϕ =yaw, θ =pitch, ψ =roll). The second feature is linear acceleration and is computed as:

$$f_2 = \frac{1}{W} \sum^W |S_{x,t}| + |S_{y,t}| + |S_{z,t}| \quad (2.4)$$

The third feature is the amount of wrist roll motion:

$$f_3 = \frac{1}{W} \sum^W |S_{\phi,t} - \frac{1}{W} \sum^W S_{\phi,t}| \quad (2.5)$$

The fourth feature is regularity of wrist roll motion. It is calculated as:

$$f_4 = \frac{1}{W} \int_W 1 \forall t \in [|S_{\phi,t}| > 10^0 \dots t + 8sec] \quad (2.6)$$

This feature takes on a value between 0 and 1. It represents the percentage of time that the wrist is in roll motion. The calculation includes the time the wrist roll is at least 10 deg/sec, plus a period of 8 sec after each occurrence of wrist roll motion falling below 10 deg/sec [8].

The study of Reyes computed another 3 features based on the same overall approach [21]. The first feature is regularity of manipulation. This feature uses a Fast Fourier Transform (FFT) to capture the regularity of peaks of smoothed manipulation. First, since the raw manipulation is noisy, the Gaussian-weighted window in Equation 2.1 was applied. The window size was $N = 225$, which is 15 seconds at a sample rate 15 Hz, with $R = 37.6$. The FFT is an algorithm that computes a Discrete Fourier Transform (DFT) but takes significantly less amount of computations than a DFT. The DFT is computed as:

$$X_k = \sum_{n=0}^{N-1} x_n * e^{\frac{-2\pi i}{N}nk} \quad (2.7)$$

where N is the number of data, each X_k is a complex number and x_n is the input

sequence. The regularity of manipulation is calculated as:

$$f_5 = \frac{1}{t} \sum_{i=LFB}^{HFB} \sqrt{r_k^2 + i_k^2} \quad (2.8)$$

where LFB and HFB represent the lower and higher frequency boundary separately, r_k and i_k are the real and imaginary parts of the index k of the FFT output using Equation 2.7, and t indicates the length of the segment in seconds. The LFB is chosen as $\frac{2}{60}$ Hz and the HFB is picked as $\frac{6}{60}$ Hz.

The second feature is called time since last EA. The idea of the time since last EA is that it is very unlikely for a person to eat again immediately after an EA [21]. The time since last EA feature is calculated as:

$$f_6 = t - t_{last} \quad (2.9)$$

where t_{last} represents the end time of the last segment classified as EA and t represents the start time of the unknown segment which is currently in the classification process.

The third feature is the cumulative eating time, which is also a time-based feature. This feature implies that a person spends a certain amount of time eating in a day [21]. The cumulative eating time records the amount of time in minutes since the beginning of recording, and is calculated as:

$$f_7 = \sum_{i=0}^t \chi_i \quad (2.10)$$

where t is the current time, and χ_i is defined as:

$$\chi_i = \begin{cases} 1 & \text{if } t \in EA \\ 0 & \text{otherwise} \end{cases} \quad (2.11)$$

All 7 of these features are used in a naive Bayesian classifier for classifying EA segments and NonEA segments. As we introduced before, the segments are determined by the peak-based segmentation algorithm. The approach to classification is to assign the most probable class $c_i \in C$, given feature values f_1, f_2, \dots, f_N . Using the naive assumption of independence of features, the classification problem can be written as:

$$c_i = \arg \max_C P(c_i) \prod_j P(f_j | c_i) \quad (2.12)$$

For our problem, only 2 classes will be used, EA (denoted as c_0) and NonEA (denoted as c_1). Therefore, probabilities are initialized as:

$$P(c_i) = 0.5 \quad i = 0, 1 \quad (2.13)$$

The probability of each feature given each class is calculated by a normal distribution model as follows:

$$P(f_j | c_i) = \frac{1}{\sqrt{2\pi\sigma_{i,j}^2}} \exp\left(-\frac{(f_j - \mu_{i,j})^2}{2\pi\sigma_{i,j}^2}\right) \quad (2.14)$$

where $\mu_{i,j}$ and $\sigma_{i,j}^2$ are the mean and variance of feature j for class i .

For features f_1, f_2, \dots, f_5 , the mean and standard deviations are needed to classify an unknown segment. Table 2.1 shows these statistics for each feature calculated by our group. The probability of each feature given each class can be computed using Equation 2.14.

The probability of feature f_6 given each class is calculated in a different way. Figure 2.5 shows the cumulative distribution function (CDF) of the time since last EA feature. Probabilities in Figure 2.5 start at 0 and end at 1.0. For an unknown

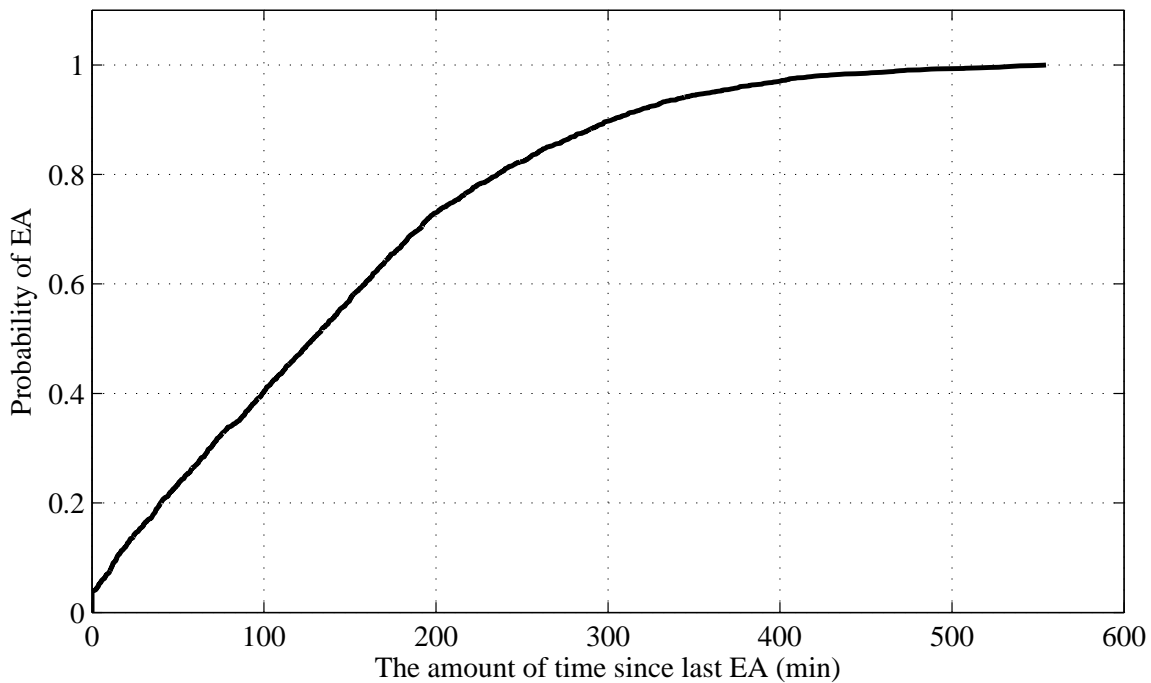


Figure 2.5: The cumulative distribution function for each minute since last EA.

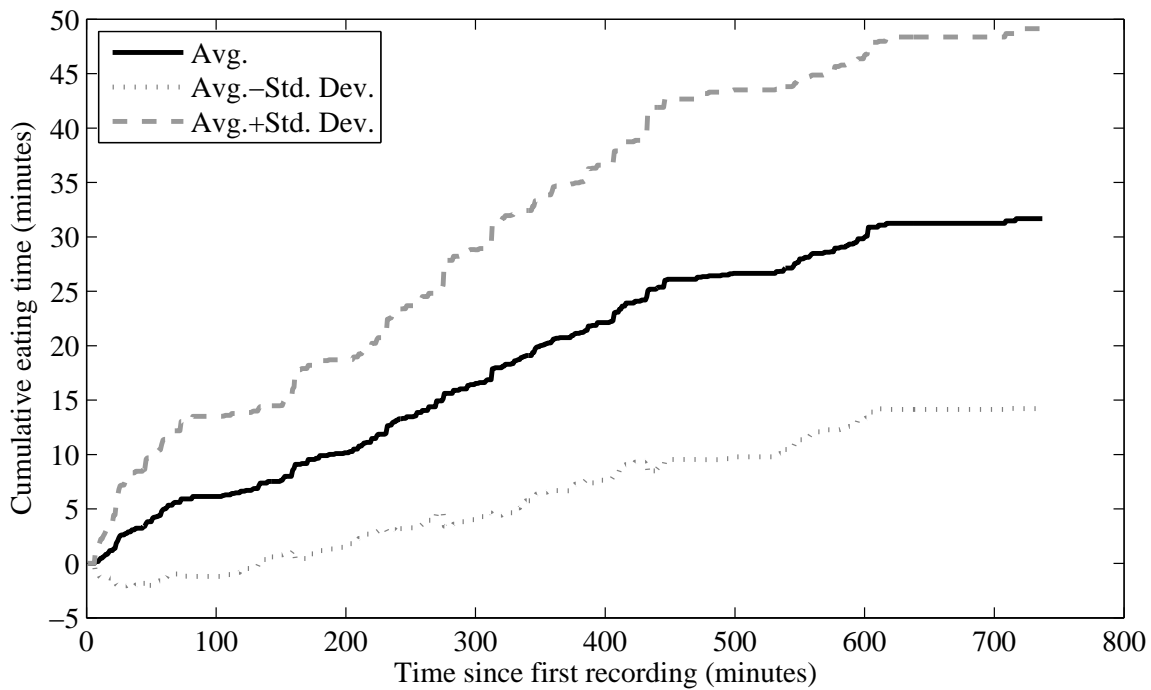


Figure 2.6: The averages and standard deviations of cumulative eating time for each minute since beginning recording.

Notation	Feature	EA		NonEA	
		Mean	Std. Dev.	Mean	Std. Dev.
f_1	Manipulation (deg/s/G)	791	214	395	239
f_2	Linear acceleration (G)	0.039	0.014	0.054	0.066
f_3	Roll motion (deg/s)	9.1	4.27	6.8	6.3
f_4	Roll regularity (%time)	0.58	0.14	0.37	0.26
f_5	Manip. regularity (deg/s ³ /G)	11654	4285	4568	2252

Table 2.1: Average feature values found during training. The values of features f_1, f_2, f_3 and f_4 were computed in [8]. The values of feature f_5 were computed independently for 2 data sets in [21]; the values given here are averaged across all data.

segment, the probability is calculated by finding the amount of time since the last segment classified as EA (minutes), and locating this value on the x -axis of Figure 2.5; the probability of this segment to be EA is considered as:

$$p(f_6|c_0) = CDF \quad (2.15)$$

$$p(f_6|c_1) = 1 - CDF \quad (2.16)$$

where CDF represents the CDF value on the y -axis. As mentioned before, EA is denoted as class c_0 and NonEA is denoted as class c_1 . If no EA has been classified prior to the current segment, Equation 2.13 is applied to set the probabilities of EA and NonEA.

The probability of feature f_7 given each class is calculated as follows. Figure 2.6 shows the average (middle line) and \pm standard deviation (top and bottom) of cumulative eating time for each minute since beginning recording. For an unknown segment, the values of μ and σ are found in Figure 2.6. The details of finding corresponding values were discussed in the study of Reyes [21]. The probability of this segment to be EA $p(f_7|c_0)$ is computed using Equation 2.14, and $p(f_7|c_1) = 1 - p(f_7|c_0)$

2.2 Data collection

An iPhone 4 [14] inside a pouch was used as the watch-like device of accelerometers and gyroscopes introduced in Section 2.1. This device was chosen because it is programmable, equipped with an accelerometer and gyroscope, and has a large memory (16GB) and battery (1420 mAh) to record data for an entire day [21].

This thesis uses 2 data sets collected previously by our group [6] [8]. Set 1 was collected using a preliminary version of the iPhone program. Users were instructed to manually log the start and end of meals/snacks. Set 2 was collected from a new version of the iPhone program on which users could press an event marker button to log the start and end of meals/snacks.

The data were collected by the iPhone program at 15 Hz. In total, 449 hours of data from 43 recordings were collected, including a total 22.4 hours of EA over 116 total meals/snacks [8]. Set 1 consists of 20 recordings and set 2 consists of 23 recordings.

For training purpose, data is segmented into EA segments and NonEA segments. EA segments simply span for the duration periods of the entire meals/snacks. For NonEA segments, the recording data is broken as 5 minutes long unless the end of the recording is reached or an EA occurs. If recording data was missed or corrupted, the recording gap was filled with zeros for all axes when the gap is less than 5 seconds, or discarded when it is longer than 5 seconds. For new features, analysis of the properties of data and calculating the statistics of features were based on the training data set. In total, set 1 consists of 35 EA segments and 1997 NonEA segments, and set 2 consists of 81 EA segments and 3201 NonEA segments [21]. We used both data sets in this thesis together without differentiating between them.

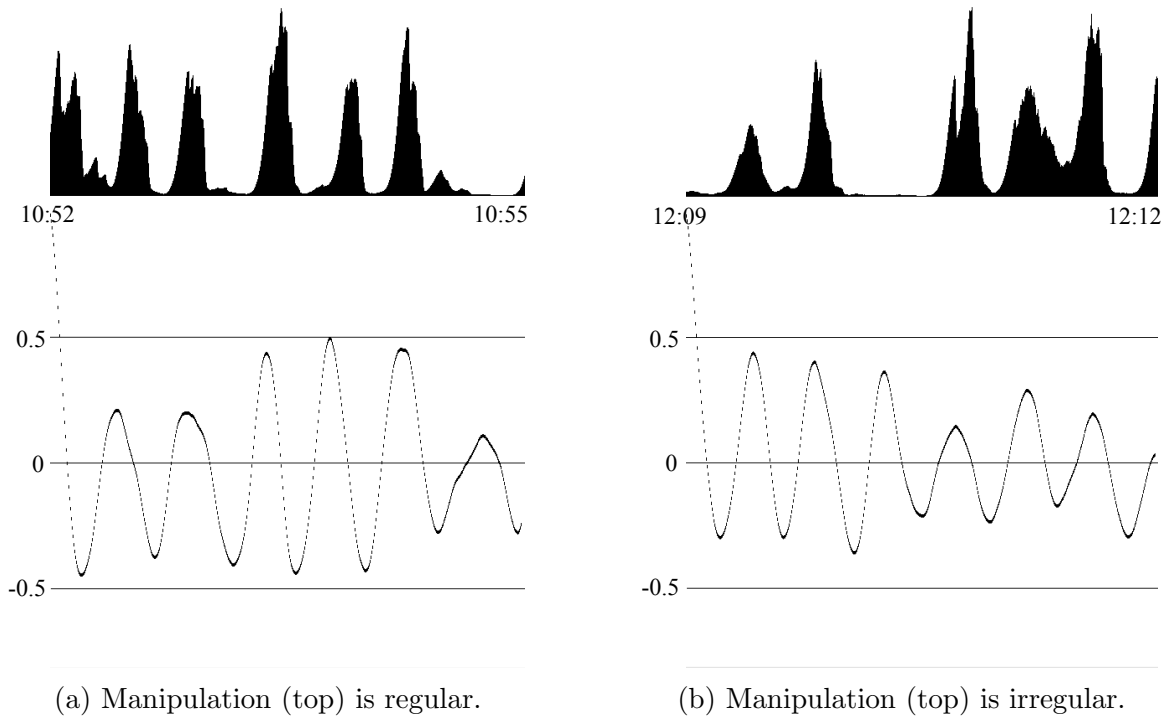


Figure 2.7: Manipulation (top) with its autocorrelation (bottom).

2.3 New features

2.3.1 Regularity of autocorrelation of manipulation

As mentioned in Section 2.1, the regularity of manipulation feature (f_5) uses a FFT approach to capture the periodicity of manipulation. The FFT algorithm uses the DFT to reduce the amount of computation [20]. The FFT converts the sampled function from the time domain to the frequency domain to enable the extraction of the dominant frequency component [2]. The FFT models the input signal as a combination of sinusoids. If the input signal is the sum of pure sinusoids, the FFT could find the periodicity in the input signal fairly well. However, the manipulation signal itself is not sinusoidal in nature, it is only regular, and manipulation may not

be regular for all eaters for all meals. People may take bites or conduct motions with irregular patterns that are only partially cyclical or have multiple phases of cycles. Figure 2.7 shows 2 examples of the manipulation. It is clear to see that the manipulation in Figure 2.7a is not sinusoidal but regular. The manipulation in Figure 2.7b is not even regular. We hypothesized that both of these problems might be addressed by taking the autocorrelation of the manipulation signal before doing a frequency analysis. As the autocorrelation results in Figure 2.7a and Figure 2.7b show, the autocorrelation signal is much more appropriate for frequency analysis.

Autocorrelation is the cross-correlation of a signal with itself. Informally, it is the similarity between observations as a function of the time lag between them [17]. It is a mathematical tool to find repeating patterns, such as the presence of a periodic signal effected by noise. Assume there are N pairs of observations on two variables x and y . The correlation coefficient between x and y is calculated by:

$$r = \frac{\sum_{i=1}^N (x_i - \bar{x})(y_i - \bar{y})}{\sqrt{\sum_{i=1}^N (x_i - \bar{x})^2} \sqrt{\sum_{i=1}^N (y_i - \bar{y})^2}} \quad (2.17)$$

where the summations are over the N observations. A similar idea could be applied on autocorrelation computation. The correlation is computed between one time series and the same series lagged by one or more time units. If the N is reasonably large, the denominator in Equation 2.17 can be simplified by approximation [18]. Finally, autocorrelation can be calculated as:

$$r_k = \frac{\sum_{i=1}^N (x_i - \bar{x})(x_{i+k} - \bar{x})}{\sum_{i=1}^N (x_i - \bar{x})^2} \quad (2.18)$$

where N is the window size, and the quantity r_k is called the autocorrelation coefficient at lag k . The variance is the average squared departure from the mean [18]. The

autocovariance coefficient is defined as:

$$c_k = \frac{1}{N} \sum_{i=1}^N (x_i - \bar{x})(x_{i+k} - \bar{x}) \quad (2.19)$$

where c_k is the autocovariance coefficient at lag k . The autocovariance at lag zero, c_0 , is the variance. Therefore, the autocorrelation at lag k can be written as:

$$r_k = c_k / c_0 \quad (2.20)$$

Since the autocorrelation is computed between the original signal and the lagged signal, the max value of lag (k) is:

$$k_{max} = Len - N \quad (2.21)$$

where k_{max} represents the max value of lag, N represents the window size, and Len indicates the length of the current data segment. The window size is chosen as:

$$N = \min(w_0, \frac{1}{2}Len) \quad (2.22)$$

where w_0 is the 2.5 minutes window at sample rate 15 Hz ($w_0 = 2250$ samples).

When a non-periodic signal is transformed using the DFT, frequency spectrum leakage occurs. The leakage causes the energy of the signal to smear out to other frequency ranges besides the actual frequency range [16]. We apply the Hanning window [12] to suppress leakage:

$$w(n) = \frac{1}{2} \left(1 - \cos \left(\frac{2\pi n}{N-1} \right) \right) \quad (2.23)$$

where N is the window size, $w(n)$ is the value of the Hanning window at the index n . The Hanning window in Equation 2.23 can be applied on the autocorrelation computed by Equation 2.18 or Equation 2.20. This is followed by performing the FFT. The new feature, regularity of autocorrelation of manipulation, is calculated as the sum of the magnitude between a range of frequencies using Equation 2.8.

Figure 2.8 shows the FFT results of the manipulation (top 2 figures)) and FFT results of the autocorrelation (bottom 2 figures) for Figure 2.7a and Figure 2.7b. We can see that for the FFT results of autocorrelation, more power focused on a smaller range of frequencies compared with the FFT results of manipulation.

We want to pick the frequency range ($[LFB, HFB]$ in Equation 2.8) that has EA and NonEA distributions separate from each other as much as possible. Two factors are defined to measure how well a given range of frequencies separates EA segments from NonEA segments [21]. The factor is calculated for EA as:

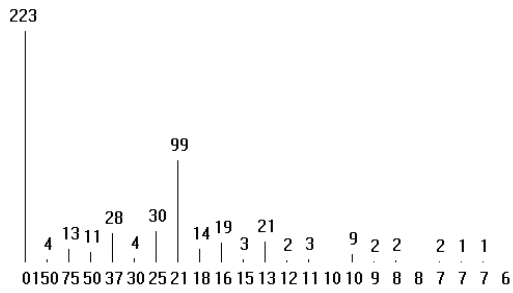
$$X_{EA} = \frac{\mu_{EA} - \mu_{NonEA}}{\sigma_{EA}} \quad (2.24)$$

and for NonEA as:

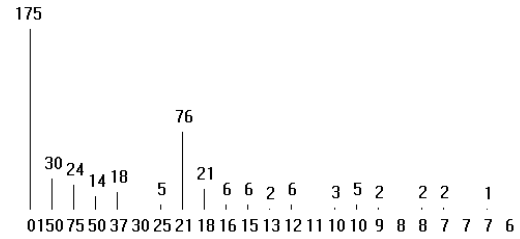
$$X_{NonEA} = \frac{\mu_{EA} - \mu_{NonEA}}{\sigma_{NonEA}} \quad (2.25)$$

where μ_{EA} and σ_{EA} are the mean and standard deviation of the EA distribution, and μ_{NonEA} and σ_{NonEA} are the mean and standard deviation of the NonEA distribution. A higher factor X means the EA and NonEA distributions are more isolated from each other.

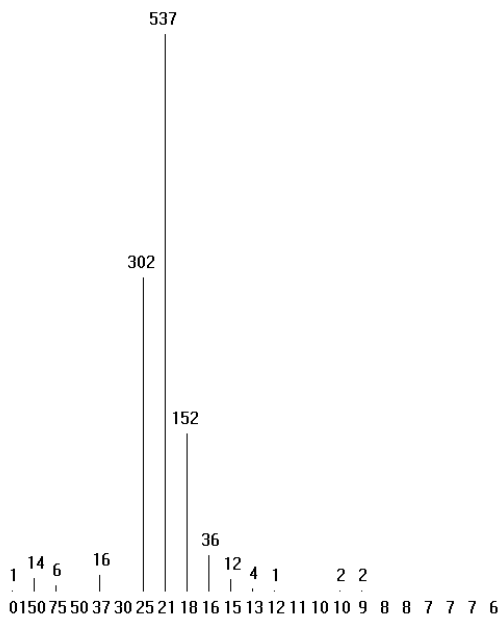
The factors values of different frequency ranges are shown in Table 2.2. Based on the results, we picked the frequency range $[\frac{3}{60}\text{Hz} - \frac{10}{60}\text{Hz}]$ since it has the highest factors overall, taking all three data set options into account.



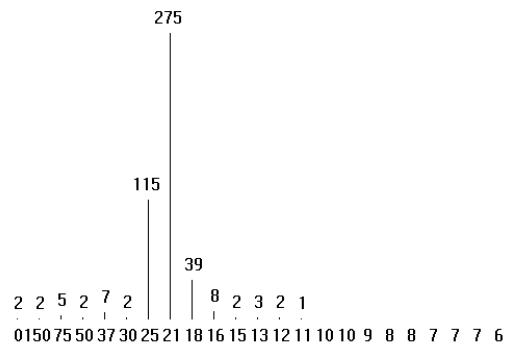
(a) FFT result of the manipulation in Figure 2.7a.



(b) FFT result of the manipulation in Figure 2.7b.



(c) FFT result of the autocorrelation in Figure 2.7a.



(d) FFT result of the autocorrelation in Figure 2.7b.

Figure 2.8: FFT results of the manipulation (top 2 figures) and FFT results of the autocorrelation (bottom 2 figures) for Figure 2.7a and Figure 2.7b. After autocorrelation, the FFT result shows a higher concentration of power in a smaller range.

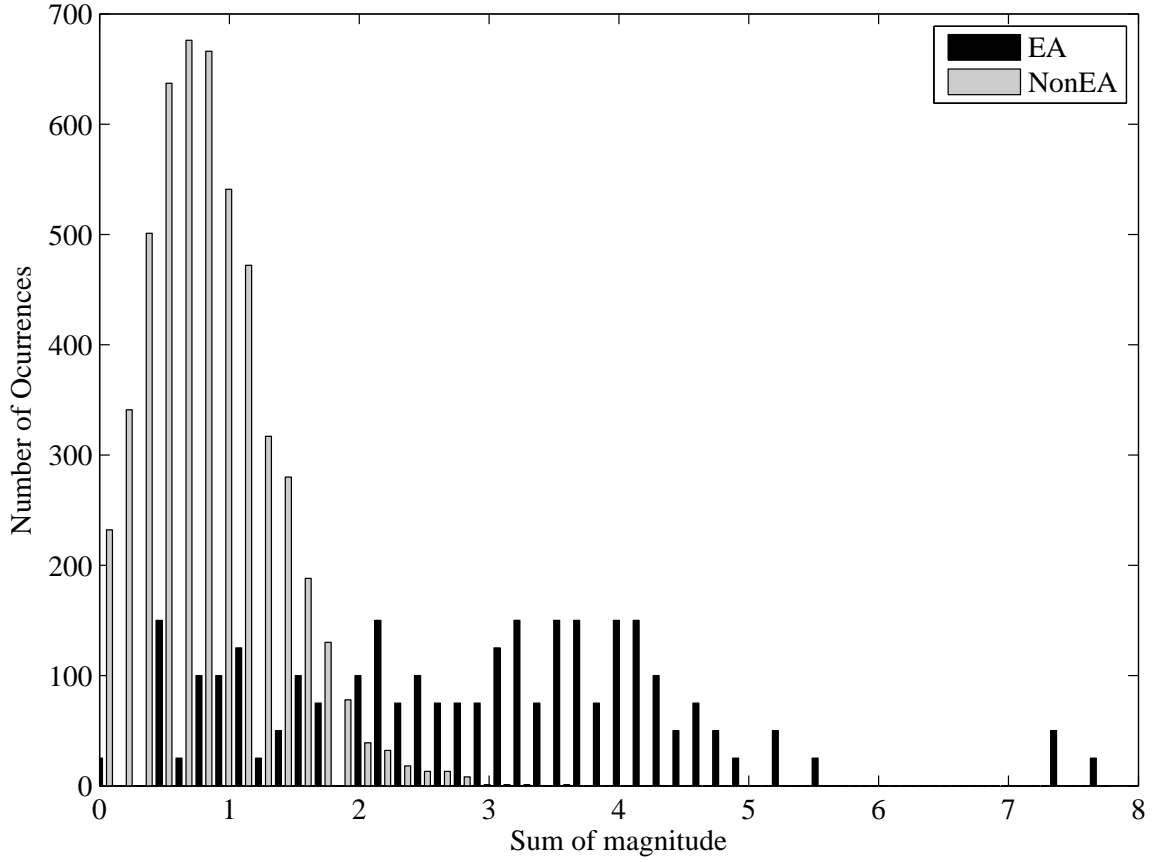


Figure 2.9: Distribution of regularity of autocorrelation of manipulation in frequency range $[\frac{3}{60}\text{Hz} - \frac{10}{60}\text{Hz}]$ (both sets).
 $X_{EA} = 1.324$, $X_{NonEA} = 4.024$.

	Set 1		Set 2		Both sets	
Range	X_{EA}	X_{NonEA}	X_{EA}	X_{NonEA}	X_{EA}	X_{NonEA}
$\frac{4}{60}$ Hz- $\frac{10}{60}$ Hz	1.311	4.014	1.253	3.765	1.271	3.829
$\frac{2}{60}$ Hz- $\frac{6}{60}$ Hz	1.242	3.633	1.244	3.676	1.243	3.659
$\frac{6}{60}$ Hz- $\frac{10}{60}$ Hz	1.375	3.779	1.002	2.858	1.098	3.130
$\frac{4}{60}$ Hz- $\frac{7.5}{60}$ Hz	1.222	3.911	1.233	3.868	1.231	3.861
$\frac{5}{60}$ Hz- $\frac{10}{60}$ Hz	1.424	3.882	1.077	3.059	1.167	3.304
$\frac{5}{60}$ Hz- $\frac{7.5}{60}$ Hz	1.277	3.843	1.053	3.236	1.116	3.415
$\frac{3}{60}$ Hz-$\frac{10}{60}$ Hz	1.359	4.263	1.308	3.931	1.324	4.024
$\frac{3}{60}$ Hz- $\frac{7.5}{60}$ Hz	1.292	4.202	1.295	4.044	1.296	4.078
$\frac{2.4}{60}$ Hz- $\frac{10}{60}$ Hz	1.380	3.920	1.268	3.814	1.298	3.841

Table 2.2: The factor values of different frequency ranges for data set 1, data set 2, and both data sets.

Notation	Feature	EA		NonEA	
		Mean	Std. Dev.	Mean	Std. Dev.
f_8	Autocorrelation regularity(/s)	2.872	1.510	0.873	0.497

Table 2.3: Statistics for regularity of autocorrelation of manipulation (both sets).

Figure 2.9 shows the distributions of EA and NonEA segments for the selected frequency range of both data sets. Since there are fifty times more NonEA segments than EA segments, the values of EA segments in Figure 2.9 are magnified by 25. Table 2.3 shows the mean and standard deviation values for the new feature, regularity of autocorrelation of manipulation. The frequency range is selected as $[\frac{3}{60}\text{Hz} - \frac{10}{60}\text{Hz}]$. The probability of this new feature f_8 given each class can be computed using Equation 2.14.

2.3.2 Time since last EA

As introduced in Section 2.1, the time since last EA feature (f_6) is a time-based feature. In the study of Reyes [21], the original method of applying this feature is the same as other non-time-based features (f_1, f_2, \dots, f_5). That means the time since last EA feature was computed as though the system ran in real-time. The method classified the current unknown segment using Equation 2.12, then moved on to the next segment. The time since last EA feature contributes to the classifier by using the CDF shown in Figure 2.5. Thus, once a segment had been classified as EA or non-EA, its class affects the feature value for subsequent segments, and it cannot be reclassified. This thesis considers the time since last EA feature in an off-line approach, trying every possible combination of classifications of segments then considering the combination with the largest sum of probabilities as the classification result.

For each combination, we calculate the sum of possibilities of each segment classified as each class. Using the naive assumption of independence of features, the probability of each segment classified as each class is calculated as:

$$p(s_k|c_i) = P(c_i) \prod_j P(f_j|c_i) \quad (2.26)$$

where s_k represents the k th segment, $P(c_i)$ is initialized using Equation 2.13. If there is an EA segment and it is not the last segment, the time since last EA feature will be used. The value of the time since last EA is found in Figure 2.5.

For example, assume $N = 3$, then all possible combinations of EA and NonEA

are:

$$\begin{array}{llll}
i_1 & NonEA & NonEA & NonEA \\
i_2 & NonEA & NonEA & EA \\
i_3 & NonEA & EA & NonEA \\
i_4 & NonEA & EA & EA \\
i_5 & EA & NonEA & NonEA \\
i_6 & EA & NonEA & EA \\
i_7 & EA & EA & NonEA \\
i_8 & EA & EA & EA
\end{array} \tag{2.27}$$

where $i_k, (k = 1, 2, \dots, 8)$ represents the row number. Assume we want to calculate the sum of probabilities of i_5 in Equation 2.27, EA is the first segment, the distance between the first segment EA (s_0) and the last segment $NonEA$ (s_2) is m , and the function in Figure 2.5 is denoted as CDF . Then using Equation 2.26, Equation 2.15, Equation 2.16 and Figure 2.5, the sum of probabilities is calculated as:

$$sum = p(s_0|c_0) + p(s_1|c_1) \cdot (1 - CDF(0)) + p(s_2|c_1) \cdot (1 - CDF(m)) \tag{2.28}$$

Recall that EA is denoted as c_0 and $NonEA$ is denoted as c_1 .

Since we only have two classes, EA and $NonEA$, the total number of possible combination is 2^N , where N is the number of segments. The average number of segments in a data recording is 67. The total possible combinations are $2^{67} - 1 \approx 1.5 \times 10^{20}$. This is a huge amount of computations, so we need to find another way of calculating the result instead of simply iterating all the possible combinations. We chose to only consider 8 segments at a time, combining the top combination iteratively as follows. First, we store all possible 256 combinations generated by 8 segments since we will use them for several times in the algorithm. Then, copy them as the initial top

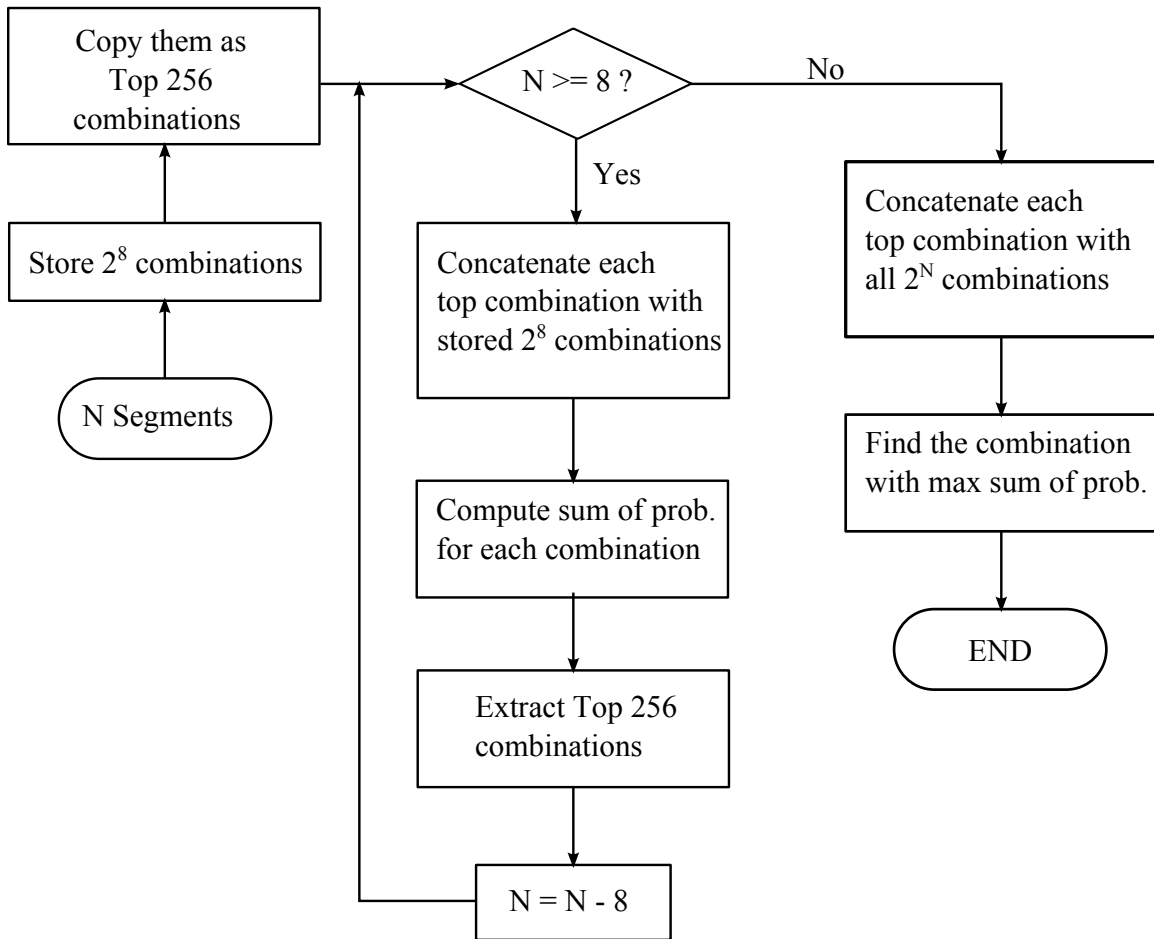


Figure 2.10: The flowchart of the algorithm of finding the combination with the max sum of probabilities.

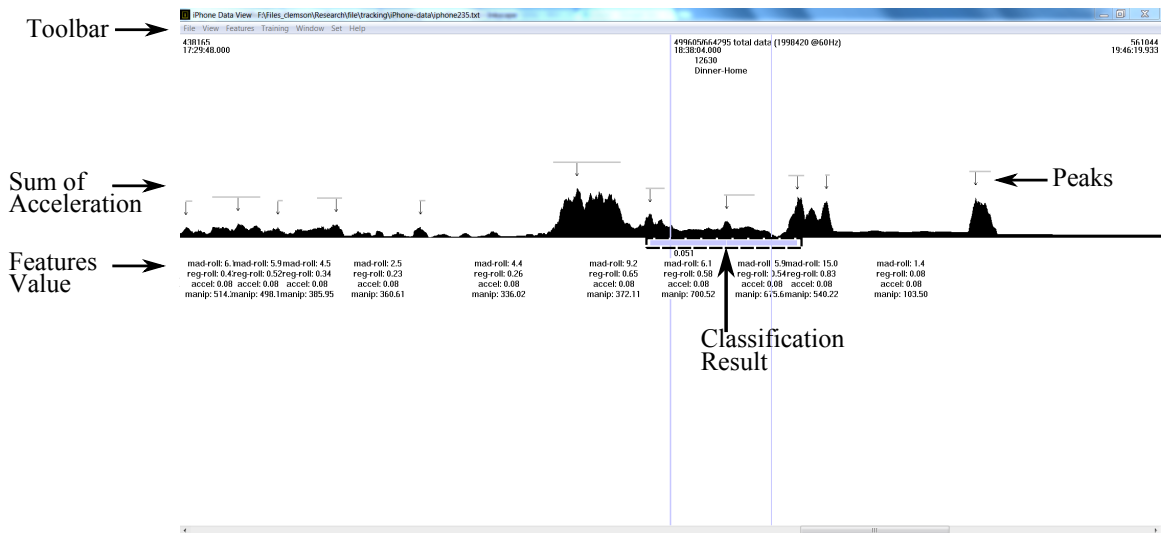
Command	Function
- +	zoom out/in
a s	rewind fast/slow
d	play/pause
f g	forward slow/fast
[]	navigate between ground truth EA
< >	decrease/increase FFT display scale
w	set autocorrelation window size
1	display smoothed manipulation
2	display smoothed manipulation and autocorrelation
3	display smoothed manipulation, autocorrelation and FFT

Table 2.4: Keyboard commands of the software tool.

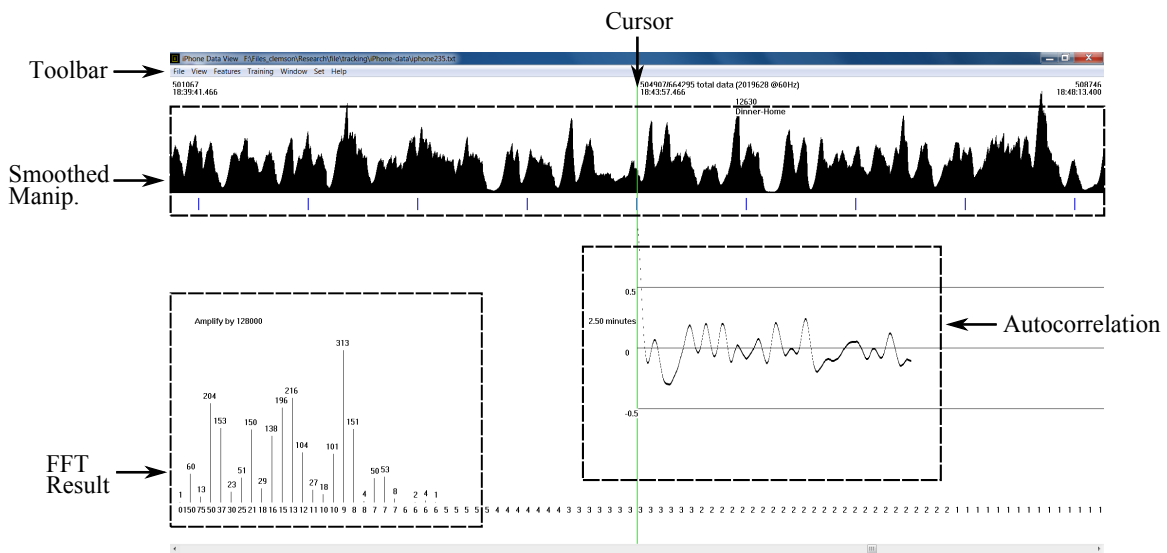
256 combinations. If remaining segments number is not less than 8, combine each top combination with stored all possible combinations, which is total $256 \times 256 = 65536$ combinations. Compute the corresponding sum of probabilities, and find the top 256 combinations with relatively higher sum of probabilities. This process repeats until the remaining segments are less than 8. Combine each top combination with all possible combinations generated by the remaining segments, and consider the combination with the largest sum of probabilities as the classification result. The flowchart of this algorithm is shown in Figure 2.10.

2.4 Software tool

A custom software tool was developed to display the ground truth, display the data, view different feature values, go through detected peaks as illustrated in Section 2.1, and perform the classification process using Equation 2.12. The keyboard commands are convenient to use and efficient to display data in any desired way, shown in Table 2.4. There are many functions of the software tool, Figure 2.11 only shows two of them.



(a) View of sum of acceleration and classification result.



(b) View of autocorrelation and FFT result.

Figure 2.11: Screenshot of the software tool.

Figure 2.11a is the view option of displaying sum of acceleration as well as the result of the Bayesian classifier. Similar to Figure 2.4, the peaks of the sum of acceleration are marked as downward arrows. The horizontal bars connected with arrows indicate the width of peaks. The values of features are displayed under the sum of acceleration. The classification results were marked as horizontal bars between the sum of acceleration and the values of features. The horizontal bars span the whole periods of the segments that were classified as EA segments.

Figure 2.11b is the view option of displaying smoothed manipulation, autocorrelation and the FFT result of the autocorrelation simultaneously. The details about autocorrelation were discussed in Section 2.3.1. Note that there is an amplify scale factor in the FFT result zone. We can turn it larger to see the frequency components that have smaller power, also we can make it smaller to have a global view of all the components.

Another software tool was developed to try every possible combination of segments, then find the combination that has the highest sum of probabilities. The details of the algorithm are shown in Figure 2.10 in Section 2.3.2.

2.5 Evaluation metrics

The metrics evaluate the classifier by the total amount of time correctly classified [8]. True positives (TP) were counted as the number of seconds of time that were labeled as EA in the manual logs and also classified as EA. False positives (FP) were counted as the number of seconds of time that were labeled as NonEA in the manual logs but classified as EA. True negatives (TN) and false negatives (FN) were computed in a similar way by comparing manual logs and classification results. The

accuracy can be calculated as:

$$accuracy = \frac{TP \times 20 + TN}{(TP + FN) \times 20 + (TN + FP)} \quad (2.29)$$

where the factor 20 weights TP to TN at a ratio of 20:1, since EA occurs much less frequently than NonEA [8]. The accuracy of EA and NonEA were computed as [21]:

$$Accu_{EA} = \frac{TP}{TP+FN} \quad (2.30)$$

and

$$Accu_{NonEA} = \frac{TN}{TN+FP} \quad (2.31)$$

Chapter 3

Results

3.1 Accuracy results

Results of the previous features which were introduced in Section 2.1 on all data are shown in Table 3.1. The values of TP, TN, FP and FN were counted in seconds. The accuracy of EA was calculated using Equation 2.30, the accuracy of NonEA was calculated using Equation 2.31, and the overall accuracy was calculated using Equation 2.29. Results of different features for each person in data set 1 are shown in Table 3.2, and results of different features for each person in data set 2 are shown in Table 3.3.

Features	Totals (sec)				Accuracy		
	TP	TN	FP	FN	EA	NonEA	Overall
f_1, f_2, f_3, f_4	61388	1266353	270261	18309	77%	82%	81%

Table 3.1: Results for previous features using average on all data [8].

Person ID	Accuracy		
	f_1, f_2, f_3, f_4	f_1, f_2, f_3, f_4, f_8	f_1, f_2, f_3, f_4, f_6
001	0.87	0.66	0.49
002	0.85	0.74	0.67
003	0.90	0.82	0.97
005	0.71	0.51	0.76
006	0.96	0.60	0.94
007	0.92	0.64	0.48
010	0.96	0.67	0.67
011	0.32	0.75	0.40
012	0.65	0.65	0.70
013	0.82	0.80	0.88
014	0.77	0.48	0.73
015	0.85	0.74	0.59
016	0.87	0.68	0.57
017	0.68	0.61	0.51
018	0.86	0.66	0.95
022	0.64	0.51	0.76
023	0.86	0.65	0.74
024	0.72	0.42	0.96
025	0.82	0.56	0.59
027	0.74	0.65	0.56

Table 3.2: Results of original 4 features (f_1, f_2, f_3, f_4) with the regularity of autocorrelation of manipulation feature (f_8), and trying every possible combination approach on the time since last EA (f_6) feature for each person in data Set 1.

Person ID	Accuracy		
	f_1, f_2, f_3, f_4	f_1, f_2, f_3, f_4, f_8	f_1, f_2, f_3, f_4, f_6
201	0.86	0.72	0.59
202	0.94	0.81	0.61
203	0.93	0.75	0.60
204	0.90	0.87	0.71
205	0.41	0.77	0.35
207	0.76	0.74	0.78
208	0.85	0.67	0.66
209	0.74	0.65	0.54
210	0.78	0.70	0.74
212	0.67	0.61	0.54
213	0.81	0.65	0.88
214	0.69	0.72	0.63
215	0.91	0.90	0.72
216	0.82	0.66	0.67
218	0.82	0.74	0.88
221	0.86	0.71	0.62
222	0.90	0.75	0.48
226	0.87	0.86	0.64
227	0.87	0.86	0.57
233	0.86	0.80	0.67
234	0.81	0.57	0.71
235	0.97	0.88	0.75
239	0.58	0.45	0.50

Table 3.3: Results of original 4 features (f_1, f_2, f_3, f_4) with the regularity of autocorrelation of manipulation feature (f_8), and trying every possible combination approach on the time since last EA (f_6) feature for each person in data Set 2.

Features	Totals (sec)				Accuracy		
	TP	TN	FP	FN	EA	NonEA	Overall
f_1, f_2, f_3, f_4, f_8	66975	863914	672700	12722	84%	56%	70%
f_1, f_2, f_3, f_4, f_6	32710	1369000	167614	46987	41%	89%	65%

Table 3.4: Results of original 4 features (f_1, f_2, f_3, f_4) with the regularity of autocorrelation of manipulation feature (f_8), and trying every possible combination approach on the time since last EA (f_6) feature.

3.2 Regularity of autocorrelation of manipulation

The results of the new feature, regularity of autocorrelation of manipulation, are shown in Table 3.4. As Section 2.3.1 described, the classifier used 5 features in total, the original 4 features (f_1, f_2, f_3, f_4) and the regularity of autocorrelation of manipulation feature (f_8). Comparing with the previous results in Table 3.1, we can see that the overall accuracy dropped from 81% to 70%. Applying the regularity of autocorrelation of manipulation, the classifier detected EA better. The accuracy of EA has been improved from 82% to 84%. However, the accuracy of NonEA decreased from 81% to 56%. The reasons why the accuracy of NonEA was not improved are explained as follows. The first reason is that, as Figure 2.9 illustrates, the distribution of NonEA is a Gaussian-like distribution while the distribution of EA does not look like a Gaussian distribution. However, when we calculate the probability of the regularity of autocorrelation of manipulation feature (f_8) given class EA (c_0) using Equation 2.14, we use a Gaussian distribution to approximate the distribution of EA. Meanwhile, the standard deviation of the EA segments is much larger than the NonEA segments, as seen in Table 2.3. These two facts cause the result that the left part of the distribution of EA overlaps with the distribution of NonEA a lot. Therefore, the classifier detected less true negatives (TN) but more false positives (FP). Although the amount of time of detected true positives (TP) was increased by 1922 seconds (about 30 minutes), the amount of time of detected false positives (FP) was greatly increased from 280915 seconds to 672700 seconds. Comparing the accuracy of the original 4 features and adding in the regularity of autocorrelation of manipulation feature to the original 4 features in Table 3.2 and Table 3.3, we can find that the regularity of autocorrelation of manipulation feature improved the classifier performance most for person ID 011 (from 32% to 75%). Figure 3.1 shows

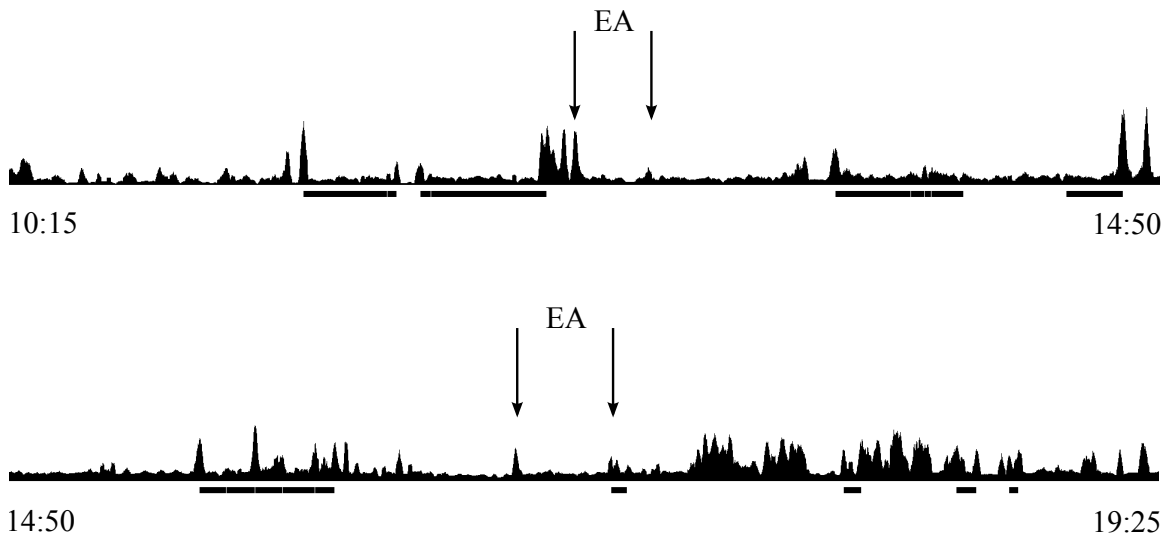


Figure 3.1: The classification results of original 4 features for person ID 011. The ground truth EA segment is marked by downward arrows. The horizontal bars represent the segments that were classified as EA segment.

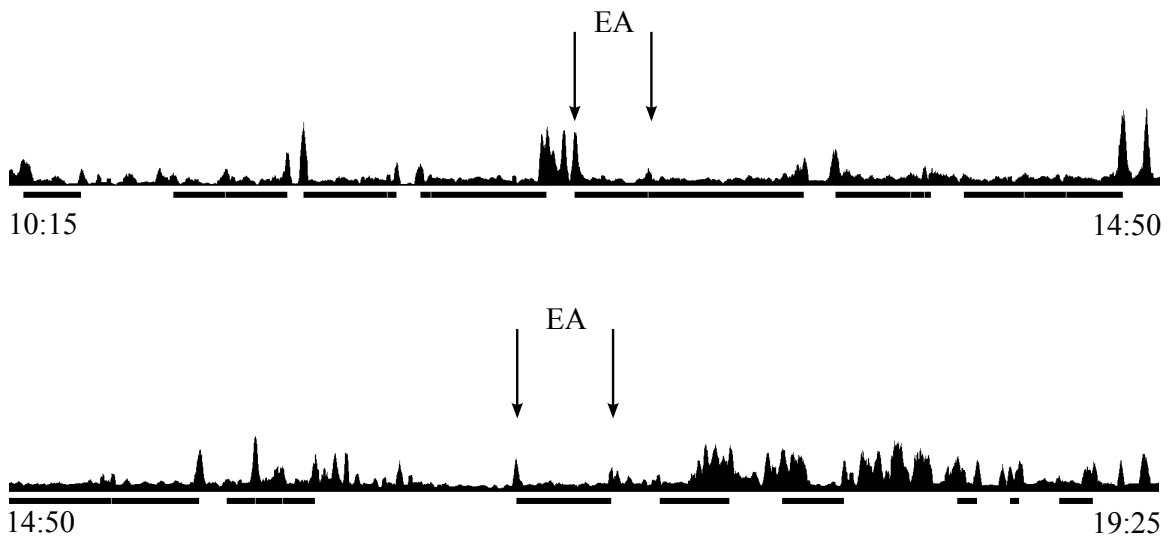


Figure 3.2: The classification results of original 4 features with regularity of autocorrelation of manipulation feature for person ID 011. The ground truth EA segment is marked by downward arrows. The horizontal bars represent the segments that were classified as EA segment.

the classification results of the original 4 features (f_1, f_2, f_3, f_4) for person ID 011, and Figure 3.2 shows the classification results of adding in the regularity of autocorrelation of manipulation feature to the original 4 features (f_1, f_2, f_3, f_4, f_8) for person ID 011. The ground truth EA segments are marked by downward arrows. The horizontal bars indicate the detected EA segments. The classifier did not detect the EA segments using only the original 4 features. After including the regularity of autocorrelation of manipulation feature, the classifier detected the EA segments correctly. We can see that although the EA segment was detected, which means the number of true positives (TP) increased, the number of false positives (FP) also increased.

Another reason for not seeing more improvement concerns the actual periodicity of the manipulation signal. As we described in Section 2.3.1, the value of the regularity of autocorrelation of manipulation feature is calculated by performing FFT on the autocorrelation of manipulation data. Figure 3.3 shows the autocorrelation of manipulation for an EA segment chosen from the area where the distribution of EA does not overlap with the distribution of NonEA (right tail of the distribution of EA in Figure 2.9). The EA segment spans 14805 samples, which is about 16 minutes at a sample rate of 15 Hz. Figure 3.3 only displays the first 5000 samples for clarity. Figure 3.4 shows the autocorrelation of manipulation for a NonEA segment chosen from the area where the distribution of NonEA does not overlap with the distribution of EA (left tail of the distribution of NonEA in Figure 2.9). As Section 2.2 illustrates, the NonEA segments are segmented into 5 minutes long. The window length is determined as 2.5 minutes (@15Hz) using Equation 2.22. Therefore, the max offset of autocorrelation is 2.5 minutes (@15Hz) after applied Equation 2.21. It is clear to see that the autocorrelation data in Figure 3.3 is much more periodic than the autocorrelation data in Figure 3.4. We can conclude that the FFT will perform really well on classifying EA segments like the one shown in Figure 3.3 and NonEA segments like

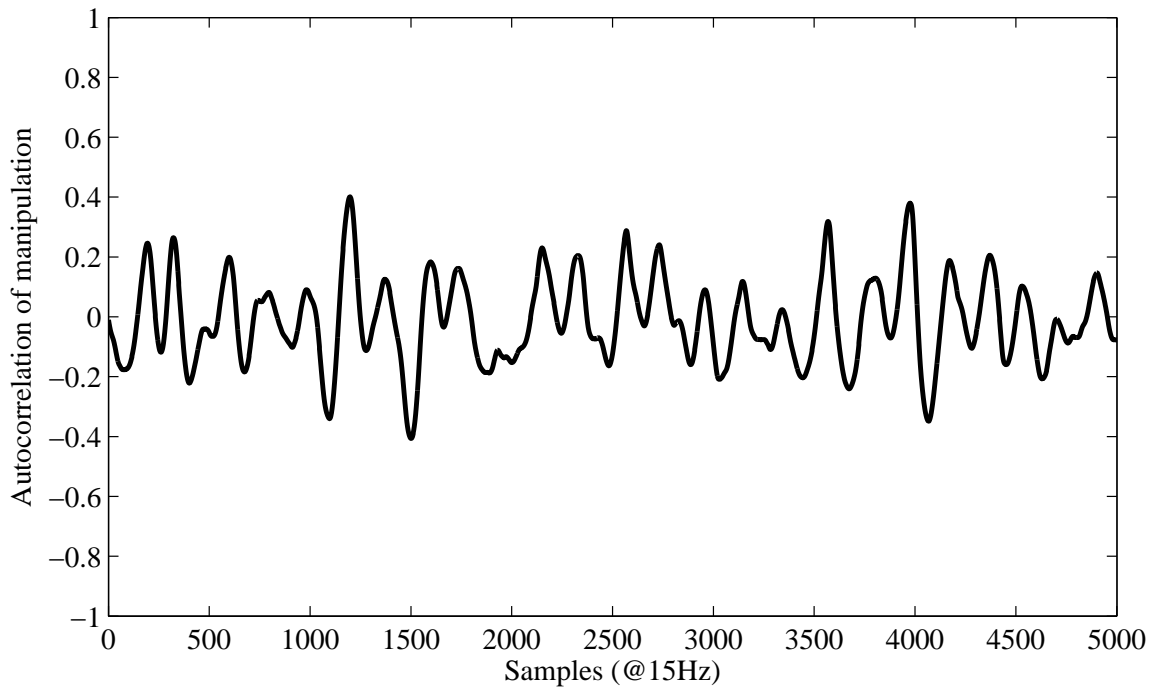


Figure 3.3: Autocorrelation of manipulation for an EA segment located on the right-most position of the distribution of EA in Figure 2.9.

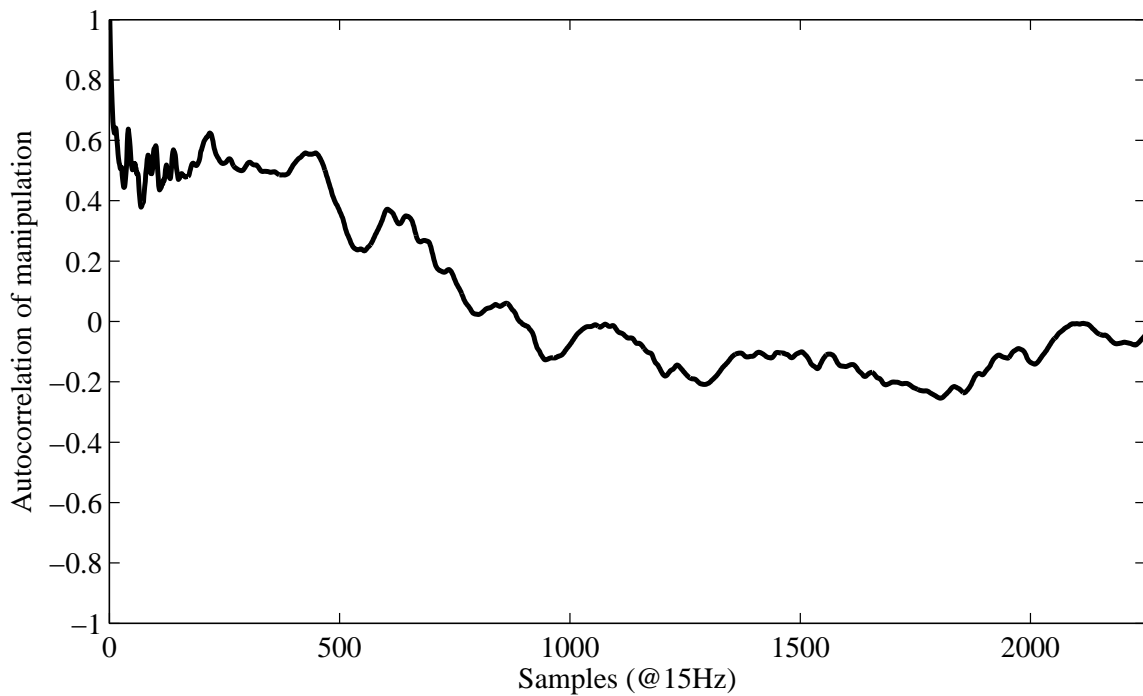


Figure 3.4: Autocorrelation of manipulation for a NonEA segment located on the left tail of the distribution of NonEA in Figure 2.9.

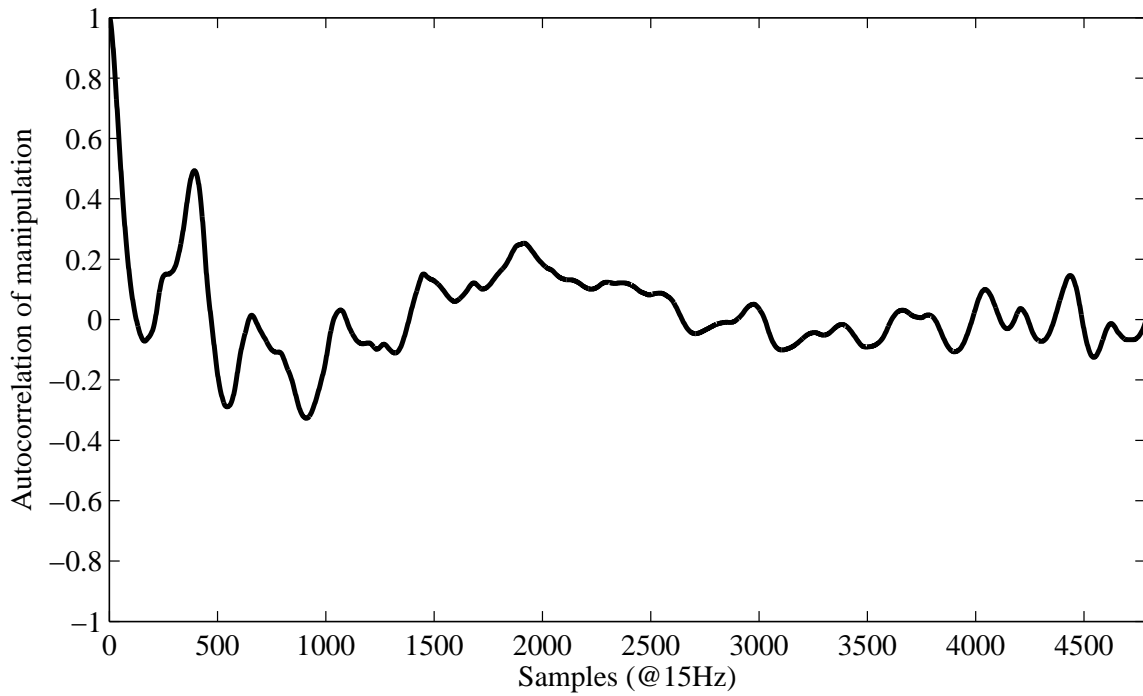


Figure 3.5: Autocorrelation of manipulation for an EA segment located in the area where the EA distribution overlaps the NonEA distribution in Figure 2.9.

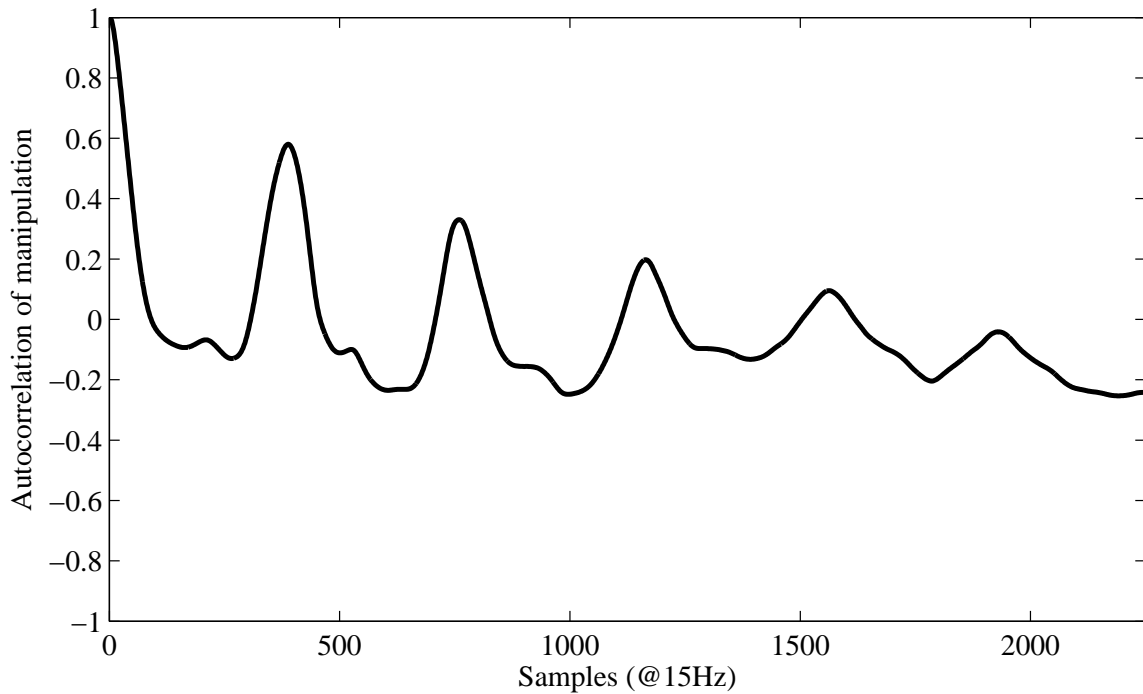


Figure 3.6: Autocorrelation of manipulation for a NonEA segment located in the area where the NonEA distribution overlaps the EA distribution in Figure 2.9.

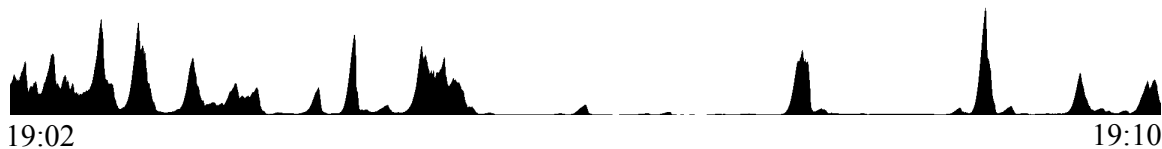


Figure 3.7: The manipulation of the EA segment in Figure 3.5.
The EA segment spans 8 minutes.

the one shown in Figure 3.4, since the autocorrelation data shows a significant difference between them. In contrast, Figure 3.5 shows the autocorrelation of manipulation for an EA segment chosen from the area where the distribution of EA overlaps with the distribution of NonEA in Figure 2.9. It is not clear to see any kind of periodicity on the autocorrelation data. Figure 3.6 shows autocorrelation of manipulation for an NonEA segment chosen from the area where the distribution of NonEA overlaps with the distribution of EA in Figure 2.9. We find that the autocorrelation data is much more periodic than the autocorrelation data in Figure 3.4.

Looking more closely at Figure 3.5, we see that the beginning part and the last part of autocorrelation show regular patterns while the middle part of the autocorrelation loses regularity. Figure 3.7 shows the manipulation of the corresponding EA segment. We can clearly see that the manipulation shows a regular pattern at the beginning part as well as the end part. The period of the manipulation signal at the right tail of the segment is approximately the same as the period of the manipulation signal at the beginning. However, the middle of the segment shows that the subject did not make manipulation motions during that time. The subject may have been doing other things like taking a rest, playing with a phone, talking to someone without moving the wrist, or drinking water by straw. Since there was a period of relatively low manipulation, the middle of the autocorrelation in Figure 3.5 shows

low periodicity.

Figure 3.8 shows another example of the autocorrelation of manipulation for an EA segment chosen from the area where the EA distribution overlaps with the NonEA distribution in Figure 2.9. Figure 3.9 shows the manipulation corresponding to the EA segment in Figure 3.8. We find that the period at the end part of the autocorrelation is clearly larger than the period at the beginning part of the autocorrelation. The subject moved frequently at the beginning of the EA, kept still for a while, then continued to move the wrist but using a slower pace than before. We are assuming that the subject pressed the start button on the iPhone program (as introduced in Section 2.1) but started to prepare another dish. The process of cooking will cause continuous manipulation. Then the subject took a rest and truly started to eat.

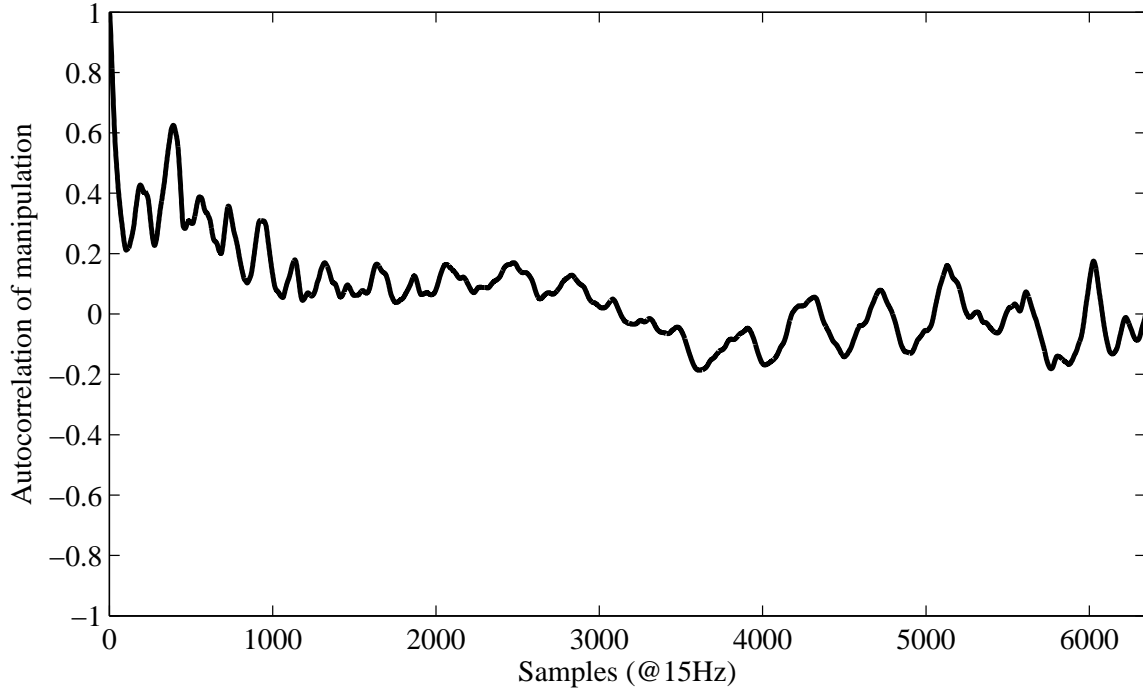


Figure 3.8: An example of the autocorrelation of manipulation for an EA segment which shows the different periodicity between the begin and the end of the segment.

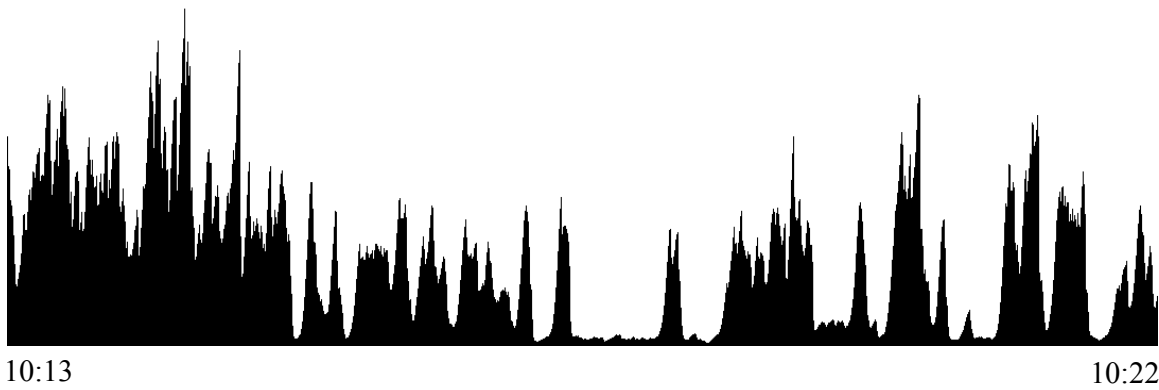


Figure 3.9: The manipulation of the EA segment in Figure 3.8

3.3 Time since last EA

The results of trying every possible combination of the time since last EA feature are shown in Table 3.4. Comparing with the previous results in Table 3.1, we find that the overall accuracy dropped from 81% to 65%. After applying the algorithm of trying every possible combination, the accuracy of NonEA was improved from 81% to 89% while the accuracy of EA decreased to 41%.

Comparing the accuracy of the original 4 features and trying every possible combination on the time since last EA (f_6) feature in Table 3.2 and Table 3.3, we find the most improvement for person ID 024 (from 72% to 96%), and the biggest decrease in accuracy for person ID 001 (from 87% to 49%). Figure 3.10 shows the classification results of the original 4 features (f_1, f_2, f_3, f_4) for person ID 024, and Figure 3.11 shows the new classification results. The ground truth EA segment is marked by downward arrows. The horizontal bars indicate the detected EA segments. Most of the FPs in Figure 3.10 are connected to each other, while after applying the method of trying every possible combination, this issue has been greatly reduced. The classifier successfully eliminated 15 FPs. Figure 3.12 shows the classification results of the original 4 features (f_1, f_2, f_3, f_4) for person ID 001, and Figure 3.13 shows the classification results of trying every possible combination on the time since last EA (f_6) feature with the original 4 features (f_1, f_2, f_3, f_4, f_8) for person ID 001. We find that although the detected EA segments are isolated with each other, they are located at the wrong times.

Recall the CDF of time since last EA in Figure 2.5 of Section 2.1. For a combination, the segments next to an EA segment will have extremely low probabilities to be classified as EA. When we are looking for the max sum of probabilities (as described in Section 2.3.2), the combination with multiple EA segments connected

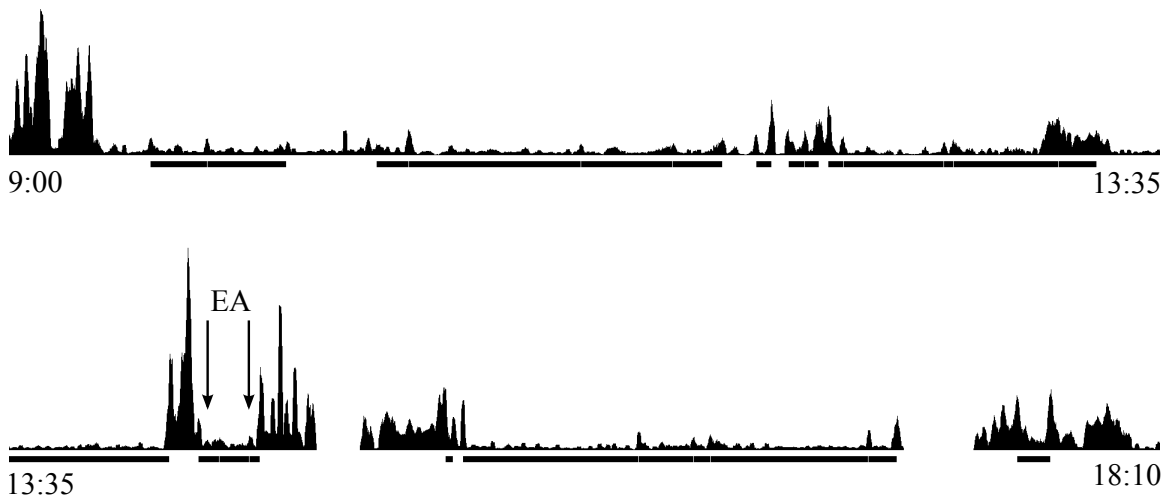


Figure 3.10: The classification results of the original 4 features for person ID 024. The ground truth EA segment is marked by downward arrows. The horizontal bars represent the segments that were classified as EA.

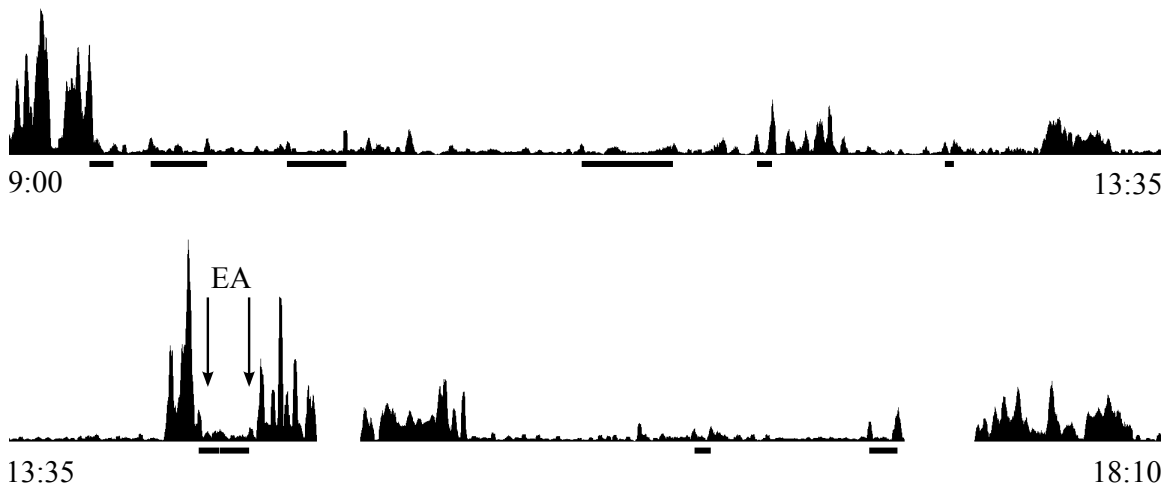


Figure 3.11: The classification results of trying every possible combination on the time since last EA feature with the original 4 features for person ID 024. The ground truth EA segment is marked by downward arrows. The horizontal bars represent the segments that were classified as EA.

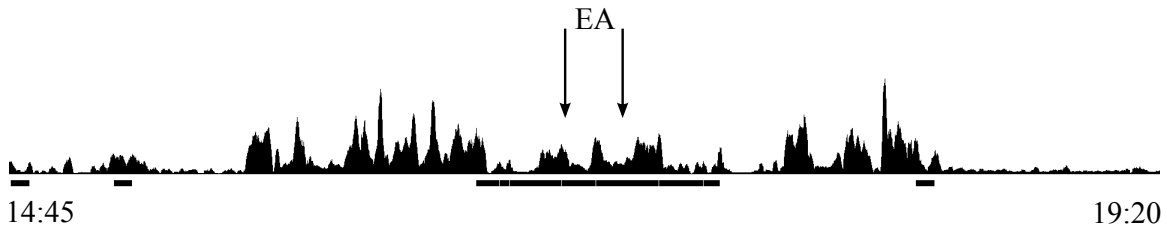
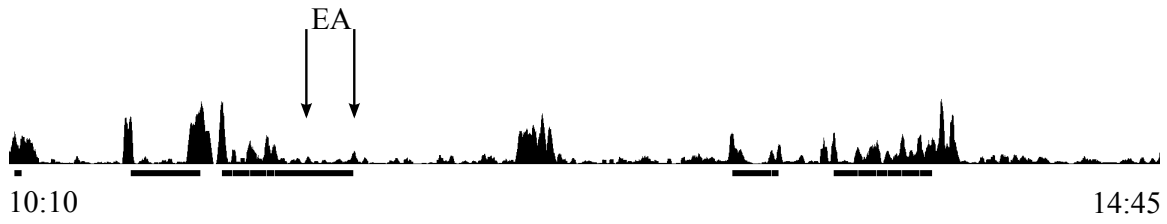


Figure 3.12: The classification results of the original 4 features for person ID 001. The ground truth EA segments are marked by downward arrows. The horizontal bars represent the segments that were classified as EA.

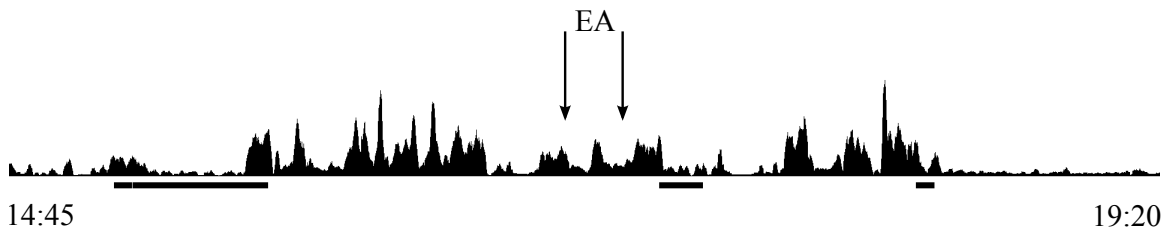
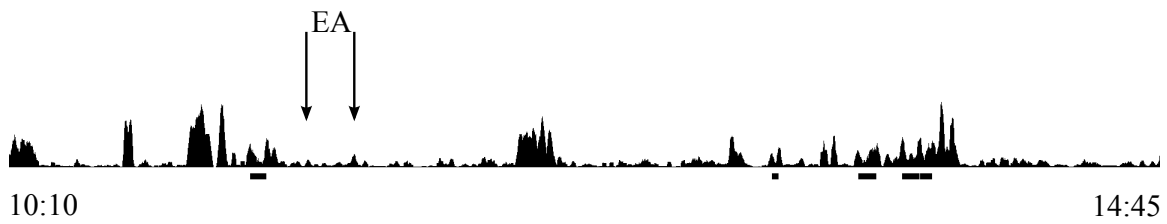


Figure 3.13: The classification results of trying every possible combination on the time since last EA feature with the original 4 features for person ID 001. The ground truth EA segments are marked by downward arrows. The horizontal bars represent the segments that were classified as EA.

is unlikely to be chosen. The chosen combination with the max sum of probabilities tends to have isolated EA segments. Therefore, the classifier detected more true negatives (TN) and suppressed false positives (FP). We can also notice that the accuracy of EA decreased from 82% to 41%. If the ground truth NonEA segment right before the ground truth EA segment has a much higher probability to be classified as EA, then the combination with the max sum of probabilities tends to choose the combination of classifying this NonEA segment as EA. Therefore, the ground truth EA segment will be classified as NonEA due to the value of the time since last EA feature.

Chapter 4

Discussion

This thesis was concerned with the problem of detecting eating activities during free-living by tracking wrist motion. It builds upon two previous studies done by our research group. This thesis explored 1 new feature and 1 new method of calculating a previously developed time-based feature. The new feature was the regularity of autocorrelation of manipulation. It was intended to better capture the cyclical nature of manipulation activities during eating, such as taking bites of food. The methods show that it provides a signal with more sinusoidal regularity, and that this in turn shows a higher concentration of power in a smaller range of frequencies. However, while using this feature in a classifier shows an improvement for some eaters in some meals, overall it showed a slight decrease in performance. We hypothesize that this is due to natural differences in the regularity of manipulation during eating. In some cases, the new feature helped overcome variations in regularity, while in other cases, the new feature is not appropriate. It may be that when people pause for lengthy periods of time, the use of a regularity-based feature decreases the likelihood of detection.

The previous study that considered time-based features applied these features

in a real-time paradigm, classifying each segment based upon the classification of previous segments. This thesis explored the time since last EA in an off-line paradigm, trying every possible combination of classifications. While this new paradigm substantially decreased false positives, it also reduced true positives so that overall performance was decreased. It is important to note that the algorithm chosen to explore this idea was limited computationally and did not truly try every possible combination. Due to the exponential number of possible combinations, a brute force approach is not practical. Future work may try a genetic algorithm that improves the search by trying the subset of combinations most likely to produce the highest overall probability, as opposed to the simple subset-approach tried in this thesis.

For future work, we suggest that new features could be explored that focus on NonEAs rather than EAs. It may be easier to identify signal characteristics that never happen during eating, and thereby exclude those periods of time before proceeding to EA versus NonEA classification. For training, the work in this thesis used all available data, which was a single day of recording for each of 43 people. Collecting free-living data from more individuals over a longer duration is suggested to be a candidate for future studies. It may be that the classifier will perform better if it is trained on data for each person separately. This could allow the classifier to capture the typical ranges of motion during eating for each individual without grouping them all together.

Bibliography

- [1] F. Bellisle, R. McDevitt, and A. Prentice. Meal frequency and energy balance. *British Journal of Nutrition*, 77(S1):S57–S70, 1997.
- [2] P. Bloomfield. Fourier analysis of time series: an introduction. *Wiley Series in Probability and Mathematical Statistics*, 1, 1976.
- [3] L. Burke, J. Wang, and M. Sevick. Self-monitoring in weight loss: a systematic review of the literature. *Journal of the American Dietetic Association*, 111(1):92–102, 2011.
- [4] T. Burrows, R. Martin, and C. Collins. A systematic review of the validity of dietary assessment methods in children when compared with the method of doubly labeled water. *Journal of the American Dietetic Association*, 110(10):1501–1510, 2010.
- [5] C. Champagne, G. Bray, A. Kurtz, J. Monteiro, E. Tucker, J. Volaufova, and J. Delany. Energy intake and energy expenditure: a controlled study comparing dietitians and non-dietitians. *Journal of the American Dietetic Association*, 102(10):1428–1432, 2002.
- [6] Y. Dong. *Tracking Wrist Motion to Detect and Measure the Eating Intake of Free-Living Humans*. Phd dissertation, Electrical and Computer Engineering Department, Clemson University, 2012.
- [7] Y. Dong, A. Hoover, J. Scisco, and E. Muth. A new method for measuring meal intake in humans via automated wrist motion tracking. *Applied psychophysiology and biofeedback*, 37(3):205–215, 2012.
- [8] Y. Dong, J. Scisco, M. Wilson, E. Muth, and A. Hoover. Detecting periods of eating during free-living by tracking wrist motion. *Biomedical and Health Informatics, IEEE Journal of*, 18(4):1253–1260, July 2014.
- [9] E. Finkelstein, I. Fiebelkorn, and G. Wang. National medical spending attributable to overweight and obesity: how much, and who’s paying? *Health Affairs*, 22(3; SUPP):W3–219, 2003.

- [10] K. Flegal, B. Graubard, D. Williamson, and M. Gail. Cause-specific excess deaths associated with underweight, overweight, and obesity. *Journal of the American Medical Association*, 298(17):2028–2037, 2007.
- [11] S. Guo, W. Wu, W. Chumlea, and A. Roche. Predicting overweight and obesity in adulthood from body mass index values in childhood and adolescence. *The American journal of clinical nutrition*, 76(3):653–658, 2002.
- [12] F. Harris. On the use of windows for harmonic analysis with the discrete fourier transform. *Proceedings of the IEEE*, 66(1):51–83, 1978.
- [13] A. Hedley, C. Ogden, C. Johnson, M. Carroll, L. Curtin, and K. Flegal. Prevalence of overweight and obesity among us children, adolescents, and adults, 1999–2002. *Journal of the American Medical Association*, 291(23):2847–2850, 2004.
- [14] Apple Inc. <http://www.apple.com/iphone/>. 2013.
- [15] M. Livingstone, A. Prentice, J. Strain, W. Coward, A. Black, M. Barker, P. McKenna, and R. Whitehead. Accuracy of weighed dietary records in studies of diet and health. *British Medical Journal*, 300(6726):708, 1990.
- [16] D. Lyon. The discrete fourier transform, part 4: spectral leakage. *Journal of object technology*, 8(7), 2009.
- [17] Nicholas C Matalas. Time series analysis. *Water Resources Research*, 3(3):817–829, 1967.
- [18] X. Meng, R. Rosenthal, and B. Rubin. Comparing correlated correlation coefficients. *Psychological bulletin*, 111(1):172, 1992.
- [19] C. Ogden, M. Carroll, L. Curtin, M. McDowell, C. Tabak, and K. Flegal. Prevalence of overweight and obesity in the united states, 1999–2004. *Journal of the American Medical Association*, 295(13):1549–1555, 2006.
- [20] R. Rao and D. Elliott. Fast transforms algorithms, analyses, applications. *Academic Press*, 1982.
- [21] J. Reyes. *A study of time-based features and regularity of manipulation to improve the detection of eating activity periods during free living*. Master thesis, Electrical and Computer Engineering Department, Clemson University, 2014.
- [22] D. Schoeller, P. Taylor, and K. Shay. Analytic requirements for the doubly labeled water method. *Obesity research*, 3:15–20, 1995.
- [23] J. Speakman. The history and theory of the doubly labeled water technique. *The American journal of clinical nutrition*, 68(4):932S–938S, 1998.

- [24] L. Terre, W. Poston II, and J. Foreyt. Overview and the future of obesity treatment. In *The management of eating disorders and obesity*, pages 161–179. Springer, 2005.
- [25] F. Thompson and A. Subar. Dietary assessment methodology. *Nutrition in the Prevention and Treatment of Disease*, 2:3–39.
- [26] N. Wellman and B. Friedberg. Causes and consequences of adult obesity: health, social and economic impacts in the united states. *Asia Pacific journal of clinical nutrition*, 11(s8):S705–S709, 2002.
- [27] W. Willett, L. Sampson, M. Stampfer, B. Rosner, C. Bain, J. Witschi, C. Hennekens, and F. Speizer. Reproducibility and validity of a semiquantitative food frequency questionnaire. *American journal of epidemiology*, 122(1):51–65, 1985.